International Summer School on Computational Quantum Materials

Posters slides

Spin-Phonon Resonances in Nearly Polar Metals with Spin-Orbit Coupling (SOC)

Authors: Abhishek Kumar, Premala Chandra and Pavel Volkov
Affiliation: Rutgers University

PRB 105, 125142 (2022)**

Funding acknowledgement

Polar Metals:
Ferroelectricity + Metallicity

$Sr_{1-x}Ca_xTiO_{3-\delta}$

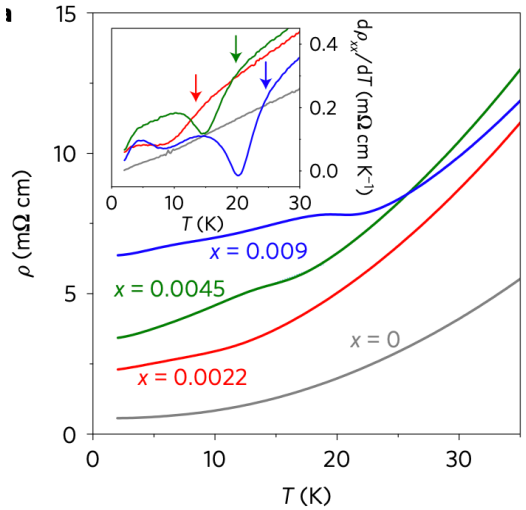

Soft modes in $Sr_{1-x}Ca_xTiO_{3-\delta}$ (STO)

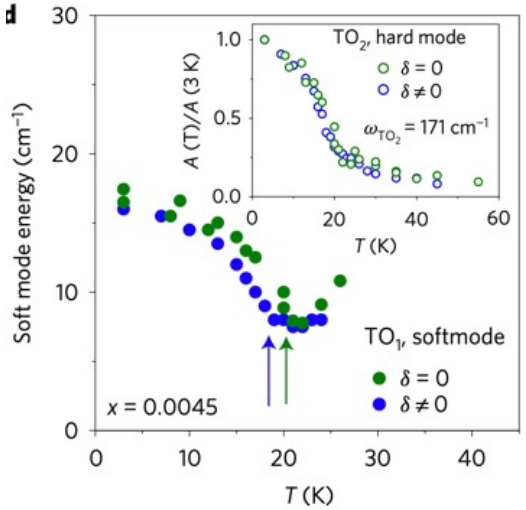

Ques: How do electrons interact with soft/critical modes in doped STO?

Spin-orbit assisted electron-phonon coupling: $H = (\mathbf{k} \times \boldsymbol{\sigma}) \cdot \mathbf{P}$

Polarization

Broken inversion + SOC ⇒ Rashba type electron-phonon interaction

No clear consensus on the strength of this coupling!!

****Motivation: To provide a way to resolve the controversy experimentally!!**

This work: Study collective modes of a polar metal in the presence of external magnetic field

Main message: Measure the energy splitting $\Delta(\lambda)$ using experimental probes and extract the coupling constant λ from analytical expression

B: Magnetic field
ω_{TO}: Soft mode frequency

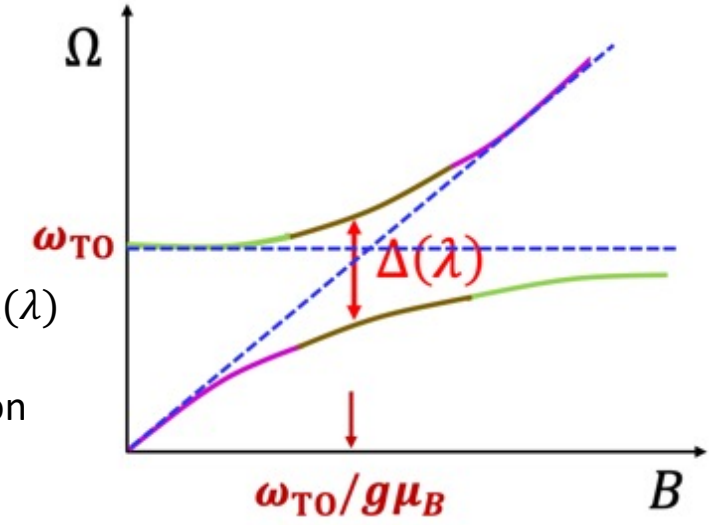

Anticrossing occurs at $B = \omega_{TO}/g\mu_B$!

Correlated Electronic Structure of Flat-Band Kagome Metal YCr_6Ge_6

Addison Richards
Department of Physics and Astronomy, McMaster University

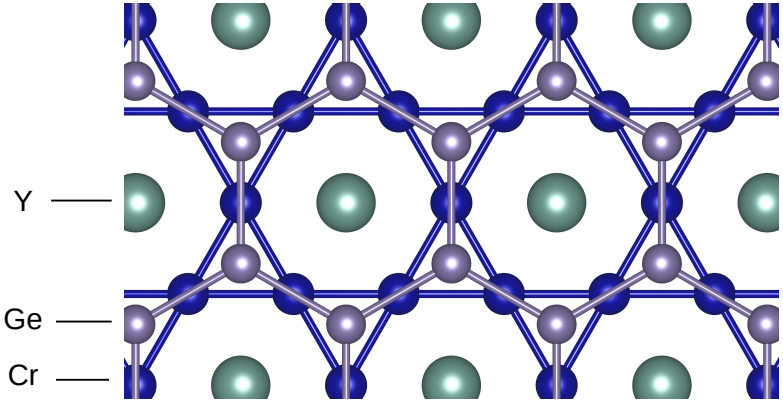

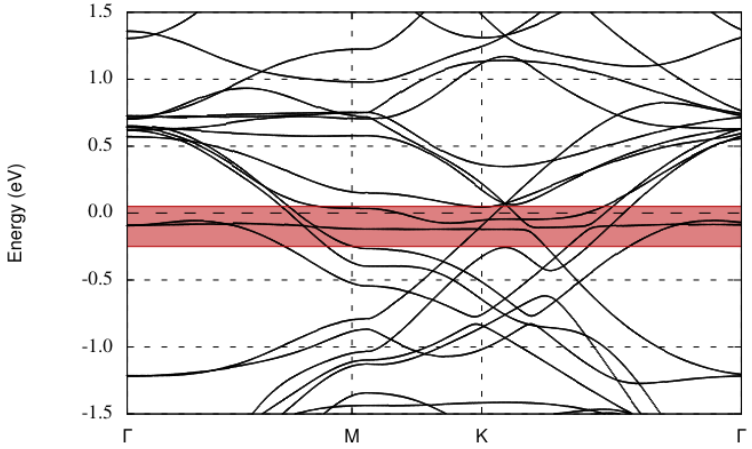

McMaster University

ETH zürich

Two routes to metal insulator transition in $SrCrO_3$

Alberto Carta & Claude Ederer

DFT+U:

Jahn-Teller distortion compatible with the AFM order

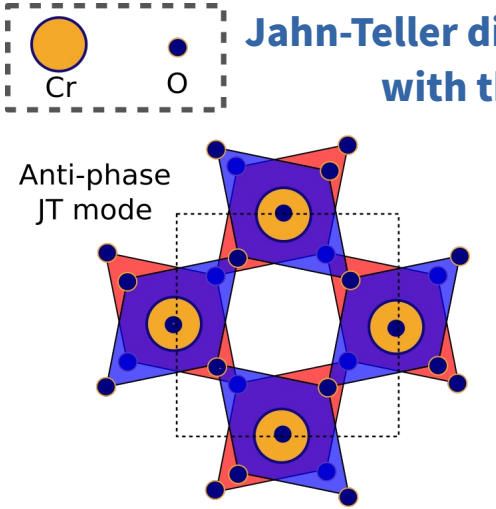

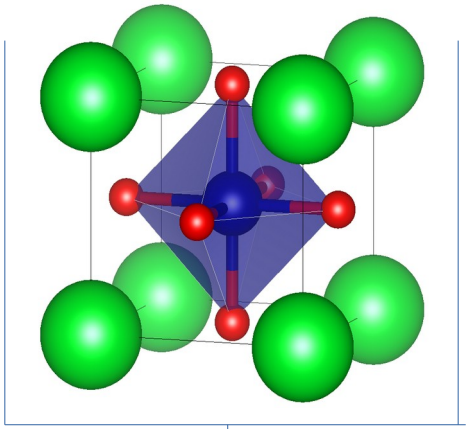

The JT mode induces G-type orbital (direction [111]) order in the C-type (direction [110]) AFM structure

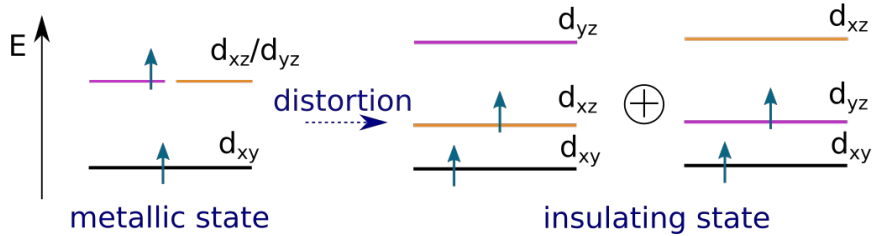

DFT+DMFT:

Breathing mode from charge disproportionation

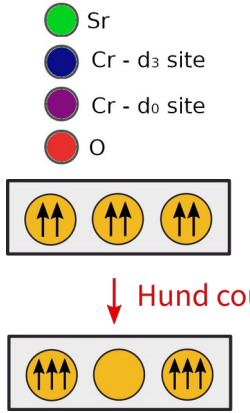

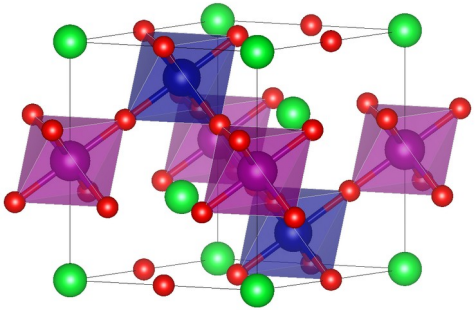

For realistic U and J value the system disproportionates and favors a breathing mode with a 3-site unit cell along the [111] direction

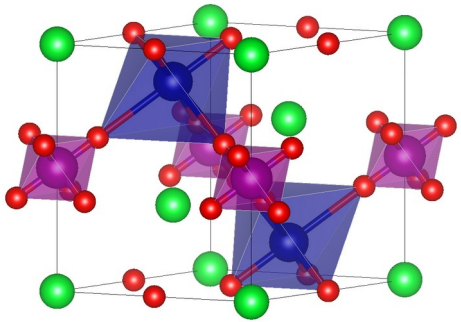

DEFECT CALCULATIONS USING A COMBINED SCAN AND HYBRID FUNCTIONAL IN γ-CsPbI3

Shengyuan Wang[1], Kin Fai Tse[1], Alena Boyko[2], Junyi Zhu[1]

[1] Department of Physics, The Chinese University of Hong Kong
[2] Department of Materials Science and Engineering, University of Toronto

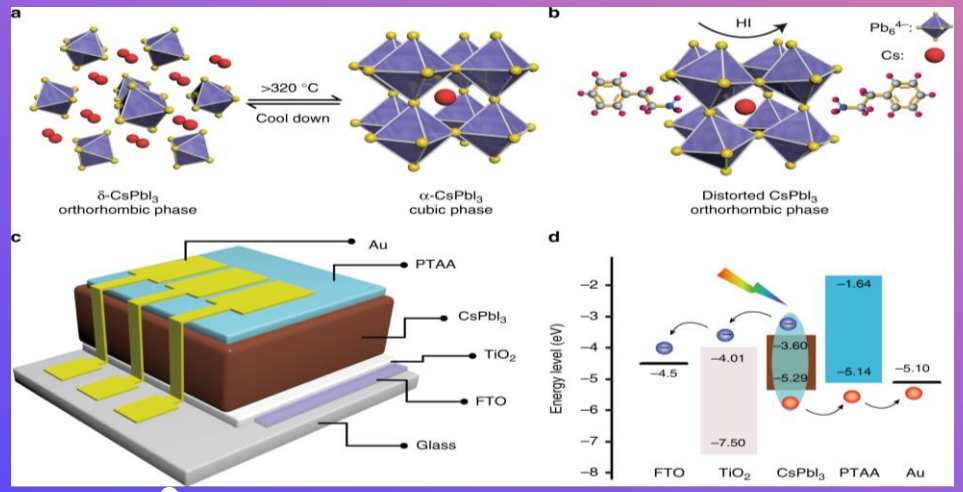

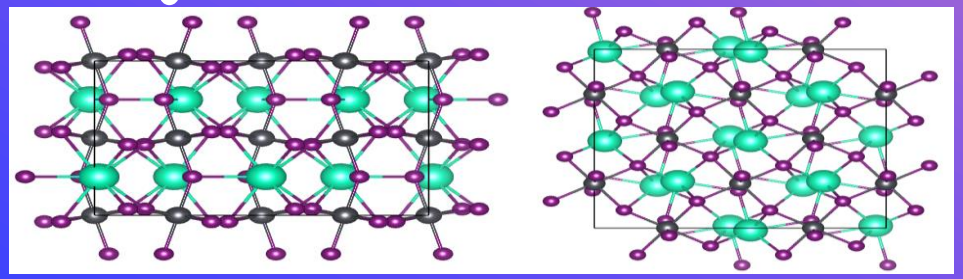

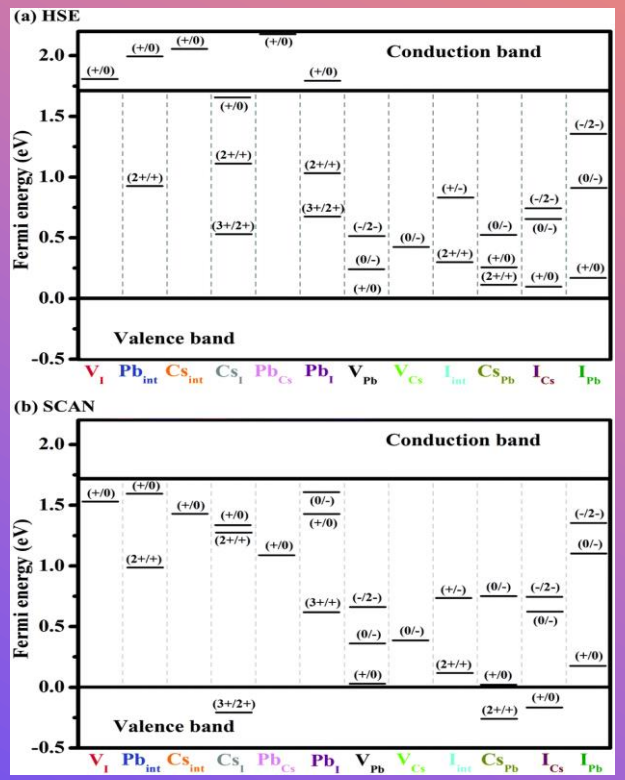

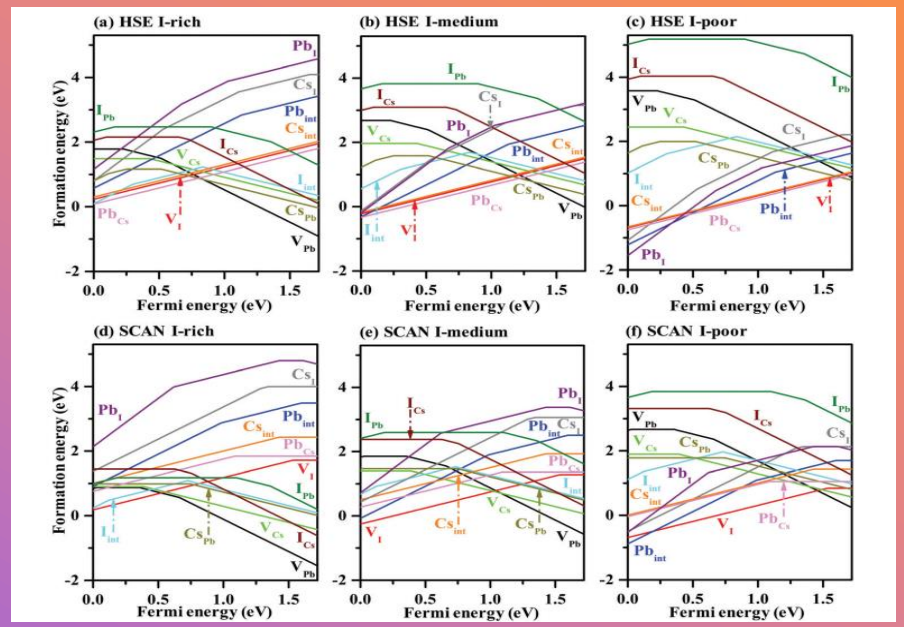

The formula for formation energy of a defect X in a charge state q is given by

$$E^f[X^q] = E_{tot}[X^q] - E_{bulk}[X^q] - \sum n_i(E_i + \mu_i) + q(E_F + \epsilon_{VBM}) + E_{corr}$$

Improved the convergence speed through a combination of structural relaxation with SCAN Meta-GGA functional and further ionic and electronic calculations with the HSE hybrid functional.

A suppressed bipolar conductivity by p-type VCs and VPb, and n-type CsI is found. Additionally, stable bipolar defects Iint and CsPb, with features of strong bond orbital coupling or structural deformation, detrimentally serve as carrier traps.

DEFECT CALCULATIONS USING A COMBINED SCAN AND HYBRID FUNCTIONAL IN γ-CsPbI3

Shengyuan Wang[1], Kin Fai Tse[1], Alena Boyko[2], Junyi Zhu[1]

[1] Department of Physics, The Chinese University of Hong Kong
[2] Department of Materials Science and Engineering, University of Toronto

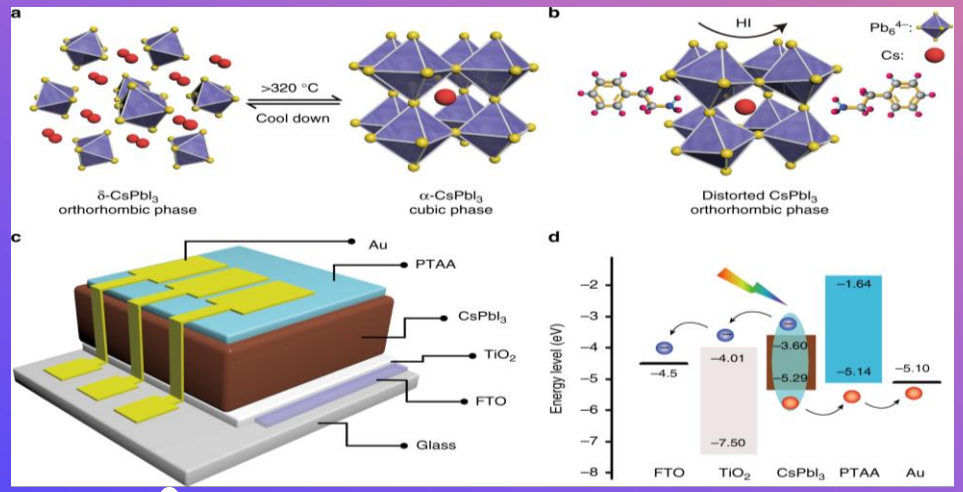

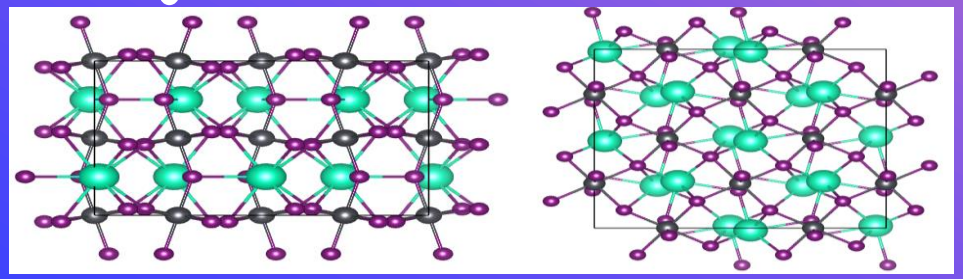

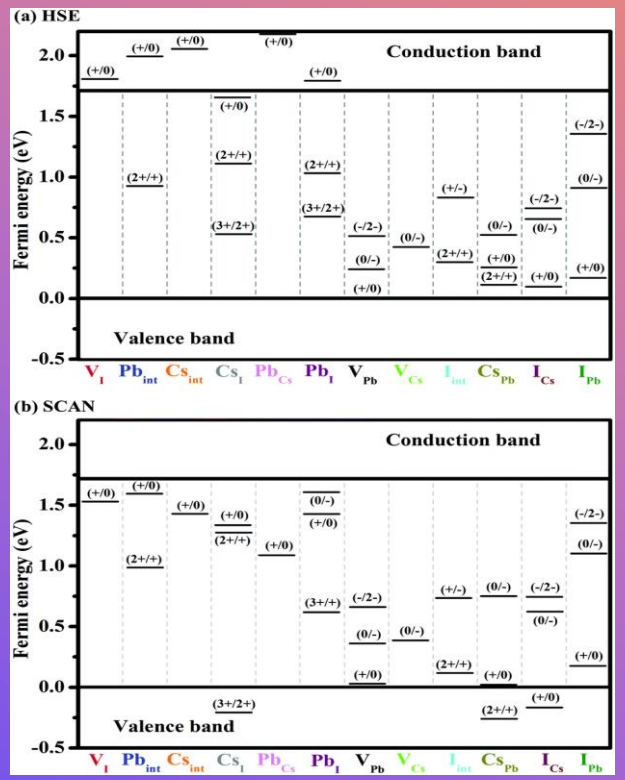

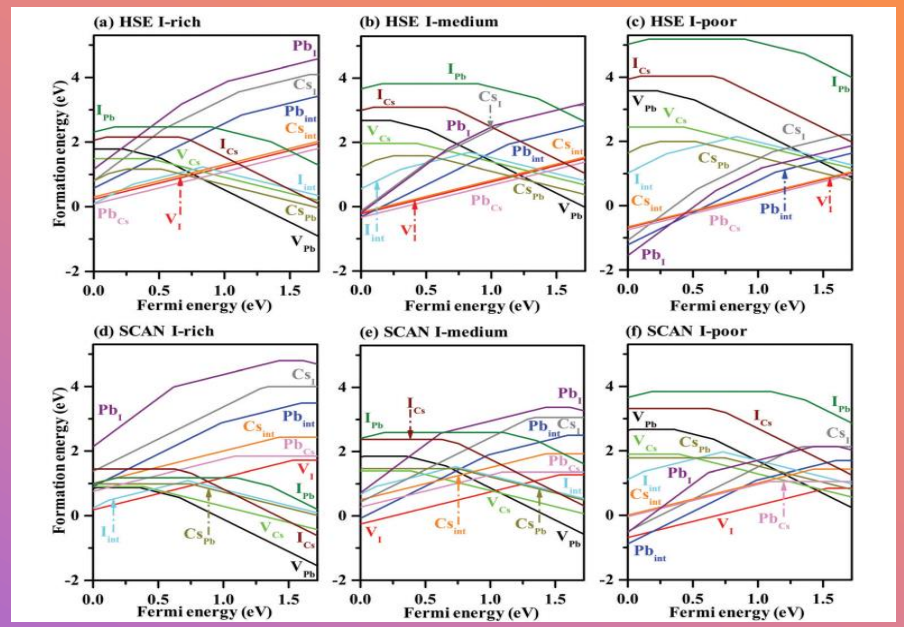

The formula for formation energy of a defect X in a charge state q is given by

$$E^f[X^q] = E_{tot}[X^q] - E_{bulk}[X^q] - \sum n_i(E_i + \mu_i) + q(E_F + \epsilon_{VBM}) + E_{corr}$$

Improved the convergence speed through a combination of structural relaxation with SCAN Meta-GGA functional and further ionic and electronic calculations with the HSE hybrid functional.

A suppressed bipolar conductivity by p-type VCs and VPb, and n-type CsI is found. Additionally, stable bipolar defects Iint and CsPb, with features of strong bond orbital coupling or structural deformation, detrimentally serve as carrier traps.

Valley polarization in biased bilayer graphene using circularly polarized light

A. Friedlan and M. M. Dignam
Department of Physics, Engineering Physics & Astronomy,
Queen's University, Kingston, ON, Canada

Introduction

There exist two inequivalent local minima in graphene's band structure known as *valleys* or *Dirac points* that are labeled K and K'. In analogy with spintronics, the valley index is binary and the concept of using this two-state system to perform logical operations is known as valleytronics. To realize such a system, we require a way to induce a *valley polarization*, that is, a differential electron population between the K and K' valleys. In this work we consider bilayer graphene, which consists of two graphene sheets stacked in an AB/Bernal stacking arrangement (see Fig. 1(a)).

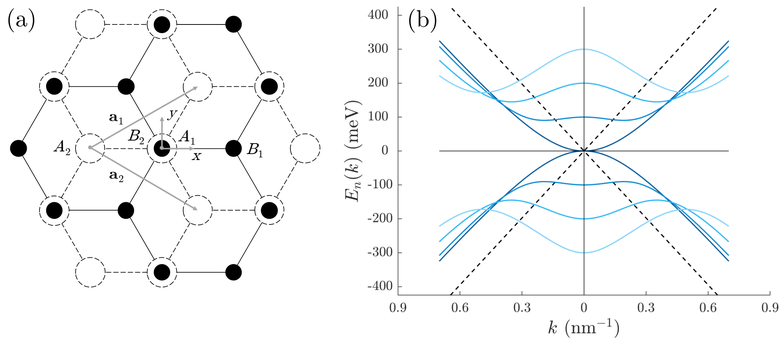

FIG. 1. (a) Bernal-stacked bilayer graphene. (b) Low-energy dispersion relation for several choices of the external bias a. From darkest to lightest, $a = 0$, 100, 200, and 300 meV.

Biasing the bilayer by applying a potential difference across the two graphene sheets breaks the inversion symmetry and opens a band gap. The band gap can be tuned continuously from zero to the mid-infrared by adjusting the strength of the external bias. It has been proposed that circularly polarized light can be used preferentially inject carriers into the K and K' valleys of bilayer graphene [1]. Right-hand circularly polarized light couples strongly to the K valley, while light of the opposite helicity couples strongly to K'. In this work, we seek to optimize the optically-induced valley-polarization with respect to the external bias and the pulse frequency [2].

Theory

We employ a four-band nearest-neighbor tight-binding model to calculate the low-energy electron bands and Bloch eigenstates of biased bilayer graphene. We perturb the system with an optical field, treating the interaction within the length gauge. The Hamiltonian is

$$H = H_0 - e\mathbf{r}\cdot\mathbf{E}(t),$$

where H_0 is the Hamiltonian of unperturbed biased bilayer graphene [3], $e = -|e|$ is the electron charge, $\mathbf{E}(t)$ is the (classical) electric field of the optical pulse at the graphene, and $\mathbf{r}$ is the electron position operator. Contained within H_0 is the external bias $2a$ between the graphene layers. The two lowest-energy bands of H_0 are shown in Fig. 1(b) for four different choices of a.

The dynamics are calculated using the Heisenberg equation of motion for the reduced density operator in the basis of the low-energy states $|n\mathbf{k}\rangle$. The matrix elements of the position operator are given by [4]

$$\langle n\mathbf{k}|\,\mathbf{r}\,|m\mathbf{k}'\rangle = i\delta_{nm}\nabla_{\mathbf{k}}\delta(\mathbf{k}-\mathbf{k}') + \delta(\mathbf{k}-\mathbf{k}')\boldsymbol{\xi}_{nm}(\mathbf{k}).$$

Near the Dirac points, the *interband* connection element between the conduction band and valence band takes the form

$$\boldsymbol{\xi}_{cv}(\mathbf{k}) = iA(a,k)\hat{\mathbf{k}} \pm B(a,k)\hat{\boldsymbol{\theta}}_k,$$

where the plus and minus signs correspond to the K and K' valleys, respectively. Here, $\mathbf{k}$ is measured from the particular Dirac point, and $\hat{\mathbf{k}}$ and $\hat{\boldsymbol{\theta}}_k$ are the standard unit vectors in polar coordinates. A and B are real and positive functions that depend only on $k = |\mathbf{k}|$ and the external bias a. For a circularly polarized pulse, the dominant (resonant) piece of the carrier-field interaction is proportional to

$$\mathbf{E}(t)\cdot\boldsymbol{\xi}_{cv}(\mathbf{k}) \sim A(a,k) \pm B(a,k),$$

where again, the plus and minus signs correspond to K and K'. When $A = B$, the above equation amounts to a valley-contrasting optical selection rule in favor of the K valley. We find this condition to be satisfied for $k = k_1$, where $k_1 = 2a\hbar/v_f$ with v_f the Fermi velocity of graphene. Thus, there exists a ring of states with radius $k = k_1$ surrounding each Dirac point where the optical selection rule becomes exact. This result seems to have gone unnoticed in the literature.

References

[1] W. Yao, D. Xiao, and Q. Niu, Phys Rev. B **77**, 235406 (2008).
[2] A. Friedlan and M. M. Dignam, Phys. Rev. B **103**, 075414 (2021).
[3] E. McCann and M. Koshino, Rep. Prog. Phys. **76**, 056503 (2013).
[4] C. Aversa and J. E. Sipe, Phys. Rev. B **52**, 14636-14645 (1995).

Selected results

We solve the resulting density matrix equations of motion up to second order in the electric field within the formalism of Ref. [4]. We calculate the electron populations n_K and $n_{K'}$ in the K and K' valleys respectively that result from the linear absorption of a right-hand circularly-polarized Gaussian pulse. We define the valley-polarization P to be the difference between the carrier densities injected around the K and K' valleys, normalized by their sum:

$$\mathcal{P} = \frac{n_K - n_{K'}}{n_K + n_{K'}}.$$

Without scattering

In Fig. 2 we plot $\log_{10}(1-P)$, that is, the deviation of the valley polarization from perfect polarization ($P = 1$) as a function of the external bias a and the central photon energy $\hbar\omega$ of the exciting pulse.

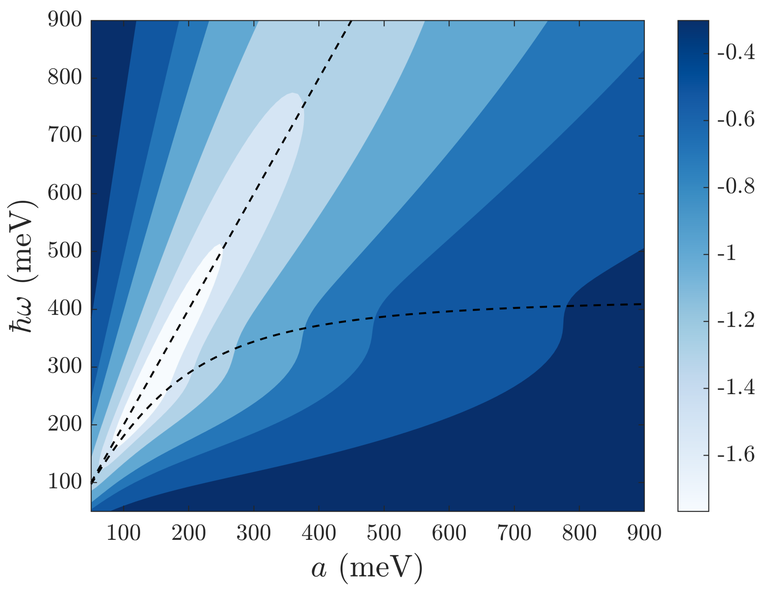

FIG. 2. Deviation of the valley polarization from perfect polarization $\log_{10}(1-P)$ as a function of the external bias a and the central frequency photon energy $\hbar\omega$ of the exciting Gaussian pulse. Lighter colours correspond to stronger valley polarizations. The three innermost contours correspond to $P = 0.97$, 0.95, and 0.90, respectively. The straight dashed line is the line $\hbar\omega = 2a$. The curved dashed line is the band gap energy. The pulse duration is 50 fs, the decoherence time is 30 fs, and the valley-polarization is evaluated long after the exciting pulse has passed. The temperature is 300 K and the chemical potential is at $\mu = 0$.

Observations

A very strong valley-polarization of over 98% can be achieved with the proper choice of frequency and bias. The strongest valley-polarizations are concentrated in the low-frequency—low-bias regime, along the line $\hbar\omega = 2a$. This occurs because $E(k_1) = a$, where $E(k)$ is the conduction band dispersion (see Fig. 1(b)). Thus, photons with energy $\hbar\omega = 2a$ will predominantly excite electrons with momentum $k = k_1$ where the valley-contrasting optical selection rule is exact.

Intervalley scattering

We now improve upon our model by accounting for intervalley scattering. In this process, an electron in (say) the K valley scatters to K' via the emission of an optical phonon. It is crucial to account for this process because it can significantly degrade the valley polarization when the frequency of the exciting pulse is large. If including intervalley scattering, one should also account for *intra*valley scattering. In this process, an excited electron loses the energy of an optical phonon but remains in its original valley. In Fig. 3 we plot the valley polarization under the same conditions as Fig. 2, but this time accounting for inter- and intravalley scattering via optical phonons.

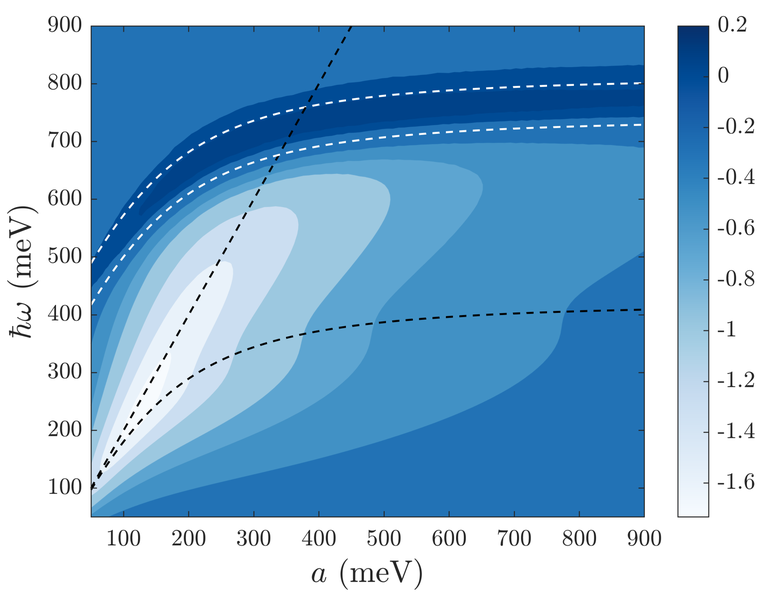

FIG. 3. Valley polarization with scattering. Lower white curve denotes the onset of intervalley scattering. Upper white curve denotes the onset of intravalley scattering.

Observations

Due to the presence of intervalley scattering, in comparison to Fig. 2, the high-frequency portion of the parameter space has been cut out from the optimal operating region. Fortunately, the low-frequency portion of the parameter space is largely unaffected by intervalley scattering since the excited electrons do not have enough energy to emit a phonon.

Thermal populations

We improve upon our model further by accounting for the thermal background of carriers present in both the K and K' valleys. In Figs. 4 and 5 we plot the valley polarization for $T = 150$ K and $T = 300$ K under otherwise the same conditions as Fig. 3.

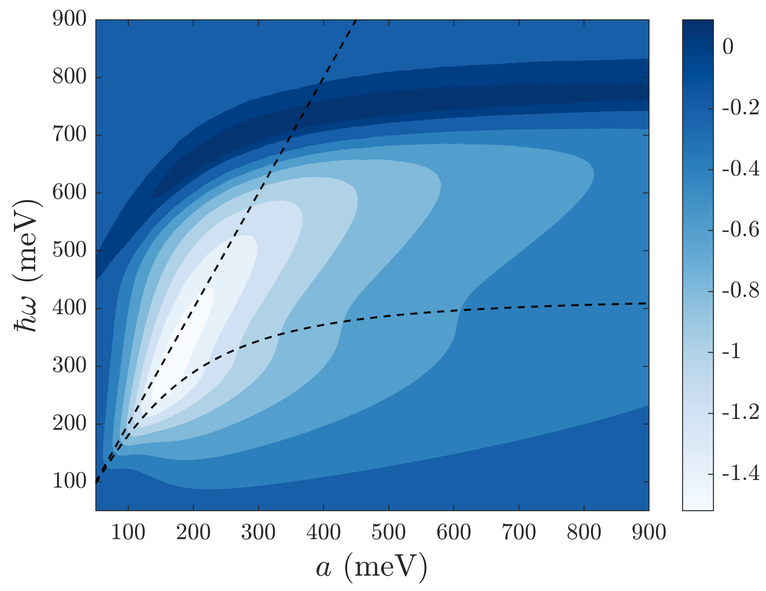

FIG. 4. Valley polarization including thermal populations and intervalley scattering. $T = 150$ K.

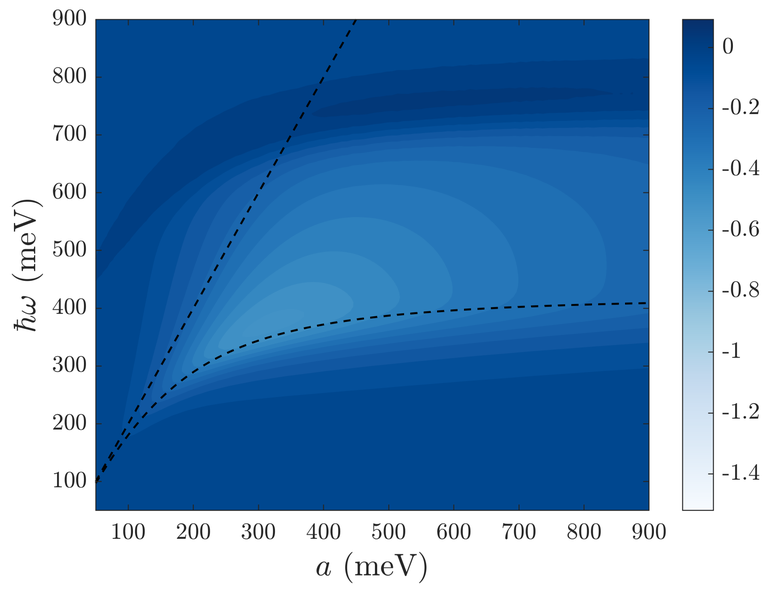

FIG. 5. As above, but for $T = 300$ K.

Observations

At 150 K, in comparison to Fig. 3, the valley polarization is reduced in the low-bias regime for which the band gap is small. However, the optimal operating region is largely unaffected. At 300 K, thermal carriers make up a significant fraction of the carrier density. The optimal operating regime has drifted away from $\hbar\omega = 2a$ and now hugs the band edge.

Figs. 4 and 5 represent our full model of valley polarization in biased bilayer graphene. In the table below we give the optimal operating frequency-bias pairs and the corresponding valley polarization.

	$T = 0$ K	$T = 150$ K	$T = 300$ K
$\hbar\omega$	235 meV	316 meV	368 meV
a	126 meV	170 meV	308 meV
P	97%	97%	70%

Conclusions

We have presented a detailed theoretical study of valley polarization in biased bilayer graphene. Our most important contributions are listed below.

- Derived condition for strong valley polarization, namely, $\hbar\omega = 2a$.
- Demonstrated how intervalley scattering destroys valley polarization at high frequencies.
- Demonstrated how thermal populations destroy valley polarization at small external biases.

With careful choice of the external bias and pulse frequency, biased bilayer graphene is an excellent candidate for valleytronic applications.

This work was supported by Queen's University and the Natural Sciences and Engineering Research Council of Canada (NSERC).

Disformal mappings of spherical DHOST geometries

Valerio Faraoni[1], Alexandre Leblanc[2]
[1]Département de physique - Université Bishop's
[2]Département de physique - Université de Sherbrooke, Institut quantique

The theoretical need to explain the present acceleration of the cosmic expansion without invoking an ad hoc dark energy keeps [1] stimulating the study of modifications of gravity with respect to Eintein's general relativity. It is quite possible that the observed cosmic acceleration is the manifestation of deviations from GR at large scales. One of the most popular candidates for modified gravity is the f(R) family of theories (where R is the Ricci scalar), a subclass of scalar-tensor gravity. However, new scalar-tensor theories of gravity have emerged and have been the subject of intense study for almost a decade, the Degenerate Higher Order Scalar-Tensor theory (DHOST) being one of them.

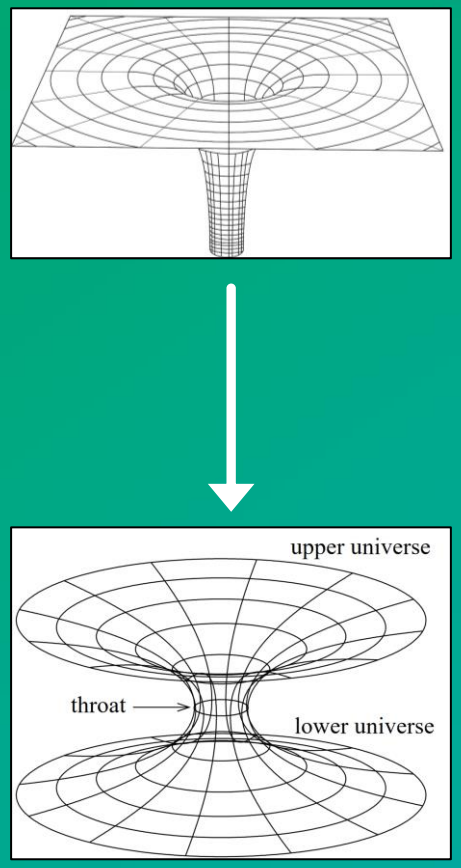

UNIVERSITÉ DE SHERBROOKE

USHERBROOKE.CA/IQ

Topological Jahn-Teller Mott insulators in twisted bilayer graphene

Andrea Blason, International School of Advanced Studies, Trieste, Italy

SISSA

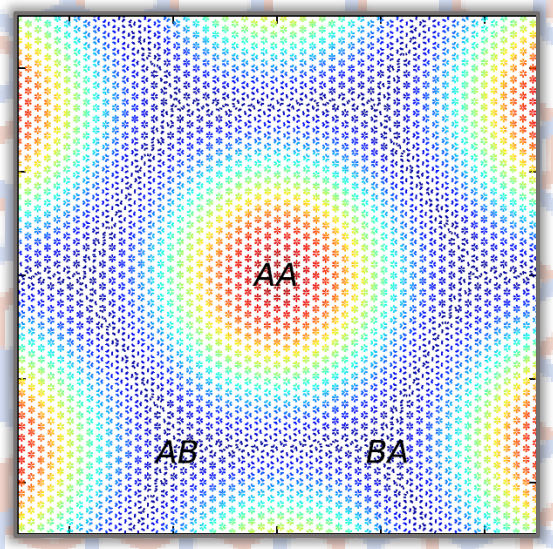

The coupling to Jahn-Teller moiré phonons overlook coulomb interaction, stabilizing mean-field insulating ground states at all integer fillings.

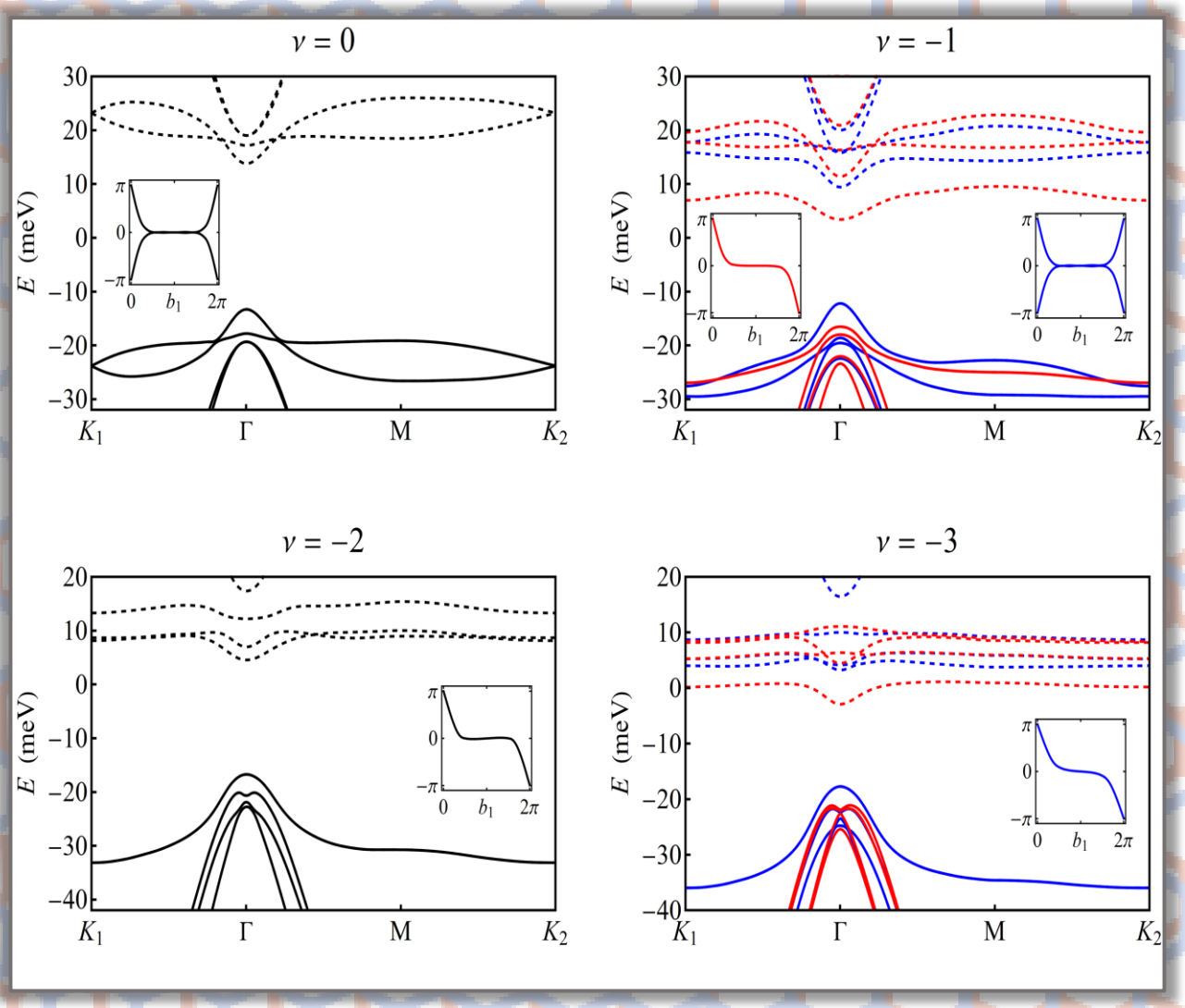

Beyond mean field, we propose a resonating valence bond state composed of topological d+id Cooper pairs, naturally prompt to superconductivity upon doping.

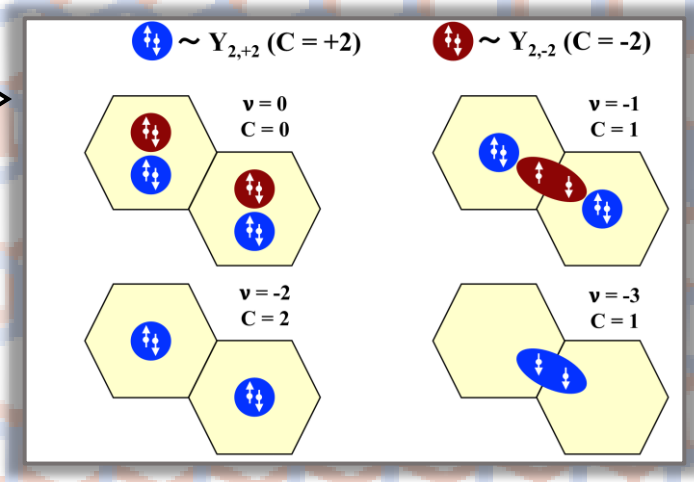

Nematic order from a multiorbital strange metal

Andrew Hardy, Arijit Haldar, & Arun Paramekanti

Abstract

- We study a two-orbital lattice extension of the Sachdev-Ye-Kitaev model in the large-N limit.
- The phase diagram features multicritical nematic ordering.
- We explore the thermodynamic, spectral, and transport properties, including the elastoresistivity.
- Our work offers a useful perspective on nematic phases and transport in correlated multiorbital systems.

The Model

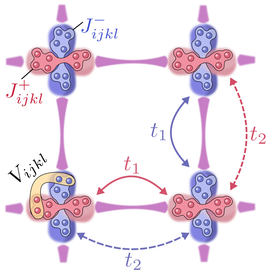

Each square lattice site ($\mathbf{r}$) is occupied by two SYK orbitals (red (+) and blue (−) circles). Each orbital has an SYK-type self-interaction ($J^{\pm}_{ijkl}(\mathbf{r})$) and an inter-orbital SYK-type interaction ($V_{ijkl}(\mathbf{r})$). Orbitals on neighboring lattice sites are connected via anisotropic hoppings with an 'easy' axis ($t_1 = t + \delta t$) and a 'hard' axis ($t_2 = t - \delta t$).

$$H_{\text{kin}} = \sum_{\mathbf{k},s,i} \varepsilon_s(\mathbf{k}) c^\dagger_{\mathbf{k},s,i} c_{\mathbf{k},s,i}$$

$$H^{\text{intra}}_{\text{SYK}} = \sum_{\mathbf{r},s,(ijkl)} J^{(s)}_{ijkl}(\mathbf{r}) c^\dagger_{\mathbf{r},s,i} c^\dagger_{\mathbf{r},s,j} c_{\mathbf{r},s,k} c_{\mathbf{r},s,l}$$

$$H^{\text{inter}}_{\text{SYK}} = \sum_{\mathbf{r},(ijkl)} V_{ijkl}(\mathbf{r}) c^\dagger_{\mathbf{r},+,i} c^\dagger_{\mathbf{r},+,j} c_{\mathbf{r},-,k} c_{\mathbf{r},-,l} + \text{h.c.}$$

arXiv:2203.11221

andrew.hardy@mail.utoronto.ca

Phase Diagram

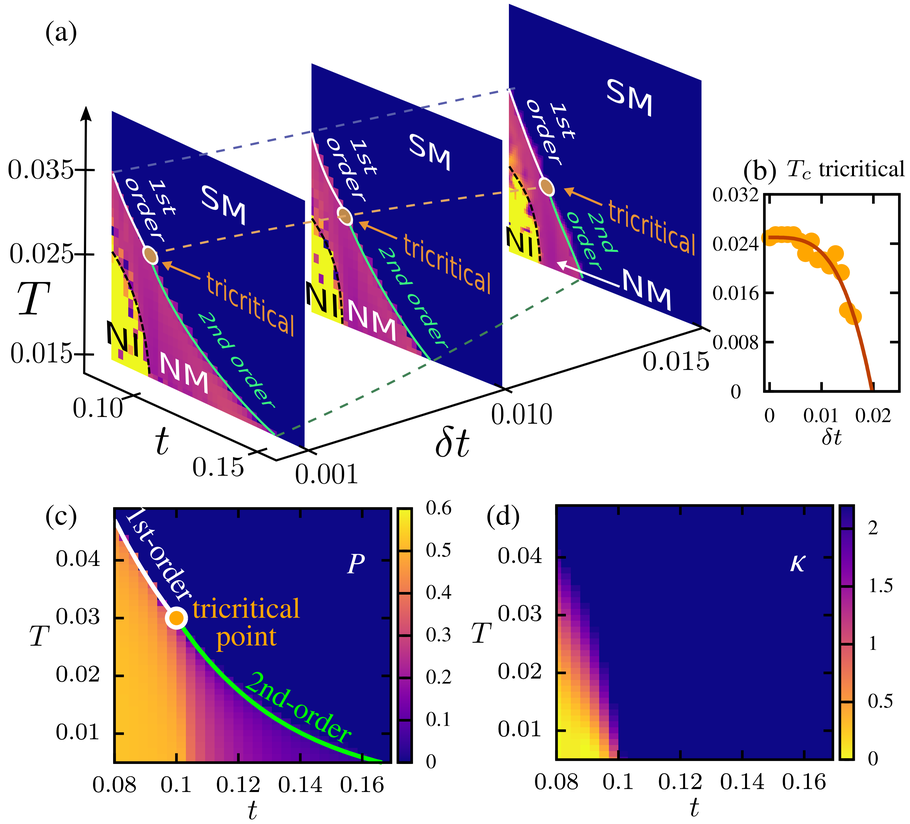

(a) Phase diagram in terms of temperature (T), hopping (t), and hopping anisotropy δt, showing an isotropic strange metal (SM), a nematic metal (NM), and a nematic insulator (NI). The isotropic and nematic phases are separated by first-order or continuous thermal transitions which meet at a tricritical point (filled circle). The NM and NI regimes are separated by a crossover at nonzero T. (b) Temperature at the tricritical point versus δt showing that it could be potentially further tuned to reach a quantum tricritical point with different strain. (c) Polarization ($P = \langle n_+ \rangle - \langle n_- \rangle$), or orbital density imbalance. (d) Compressibility ($\kappa = \langle n \rangle^{-2} \partial \langle n \rangle / \partial \mu$), distinguishing metallic from insulating phases.

DISCUSSION

- This model features a high temperature strange metal which undergoes a first-order transition into a nematic insulator or a continuous transition into nematic metal phase, separated by a tunable tricritical point.
- These phases arise from spontaneous partial polarization of the multiorbital non-Fermi liquid.
- The d.c. elastoresistivity exhibits a peak near the nematic transition.
- Additional strain effects connect to putative nematic quantum critical points.

Transport

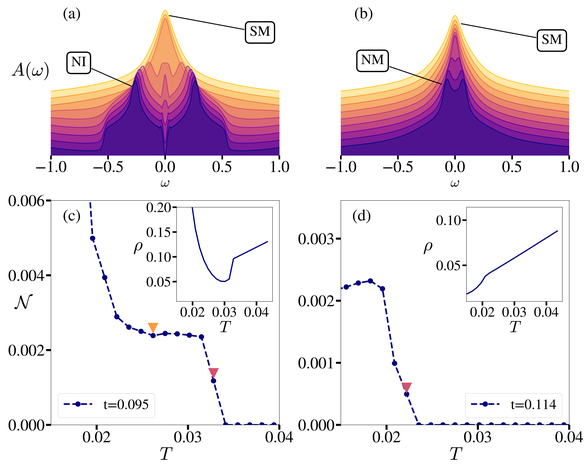

Evolution of spectral function $A(\omega)$ with temperature T as a function of frequency ω. Resistive nematicity $\mathcal{N} = (\rho_{xx} - \rho_{yy})/(\rho_{xx} + \rho_{yy})$ which is zero in the SM phase, increases and saturates in the NM, and further rapidly increases at low T in the NI regime. Inset shows the average resistivity $\rho(T) = (\rho_{xx} + \rho_{yy})/2$.

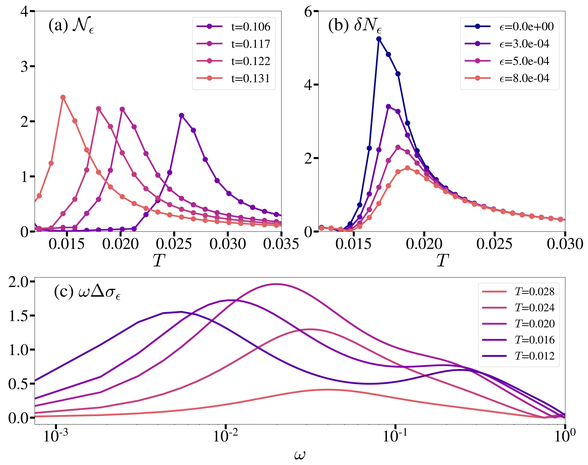

$\mathcal{N}_\epsilon(T) = (\delta\rho_{xx} - \delta\rho_{yy})/\epsilon$ is the anisotropic elastoresistivity ; the peaks correspond to T_c. (b) Strain dependence of $\delta\mathcal{N}_\epsilon(T)$ showing that the transition and hence $\delta\mathcal{N}_\epsilon(T)$ gets rounded with increasing strain. (c) $\omega\Delta\sigma_\epsilon(\omega)$ versus frequency where $\omega\Delta\sigma(\omega)$ is the anisotropic elastoconductivity,

Memory Function Formalism for the Electrical Conductivity of Periodic Systems

Brett Green

Penn State University

Mobility of the-electron gas

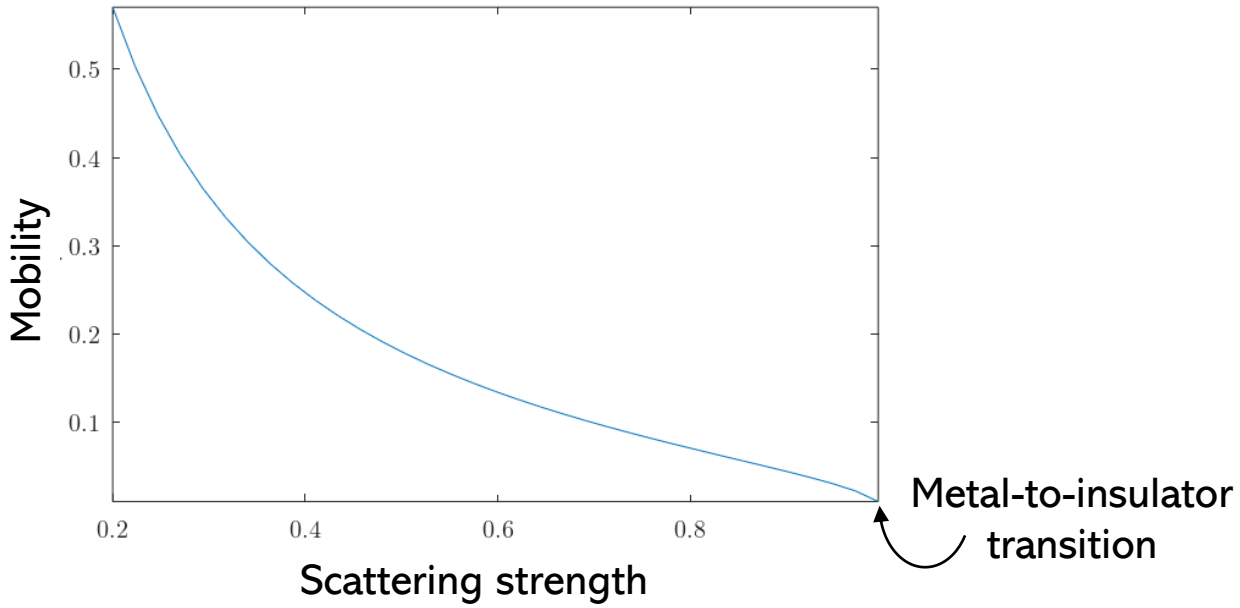

Intraband and interband mobility in graphene

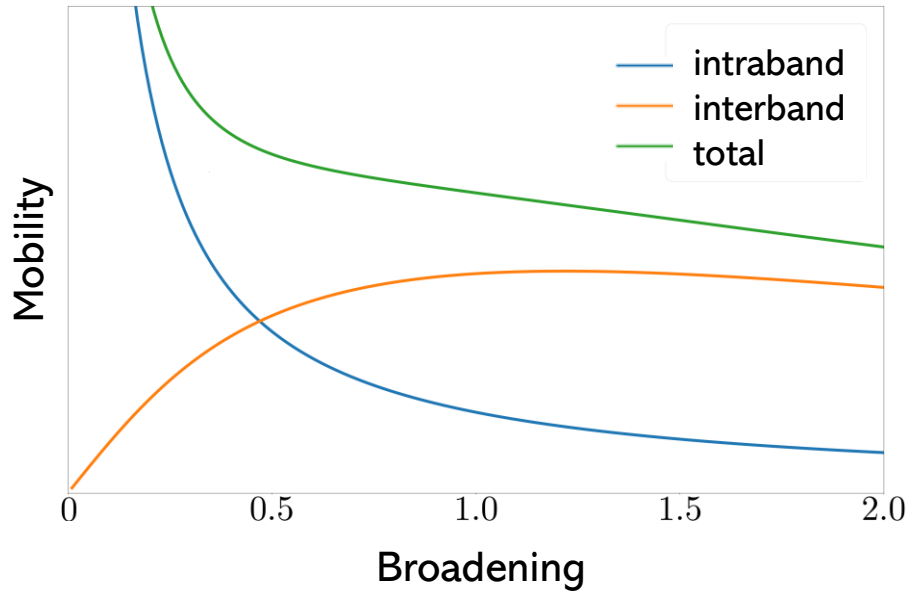

DIAG-MC MEETS QODB

JOHN POOLEY

- Stochastic sampling of Feynman diagrams
- Calculate G to obtain observables
- Perturbative/Non-Perturbative
- Exotic phases close to QCP
- Second order fluctuations reduce free energy
- Entropic stabilisation of phases

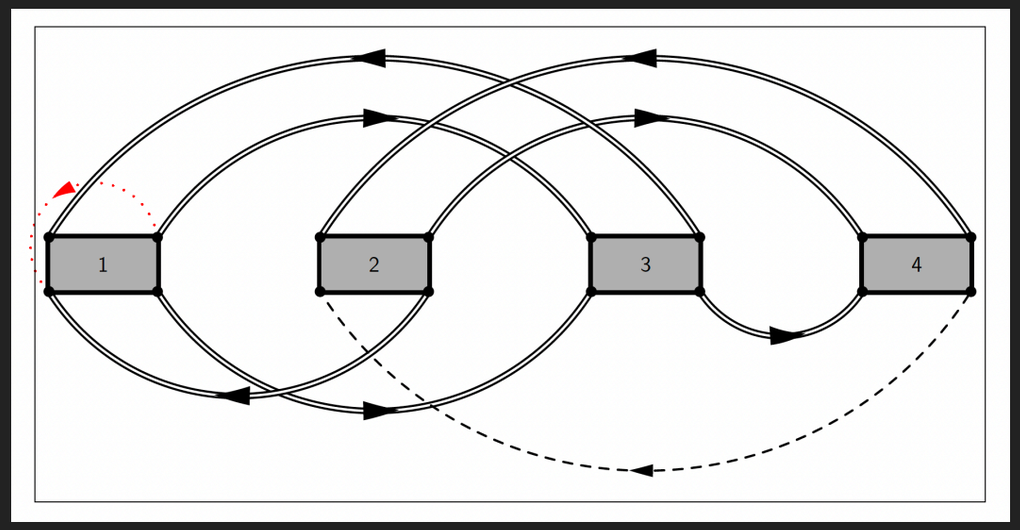

University of Kent

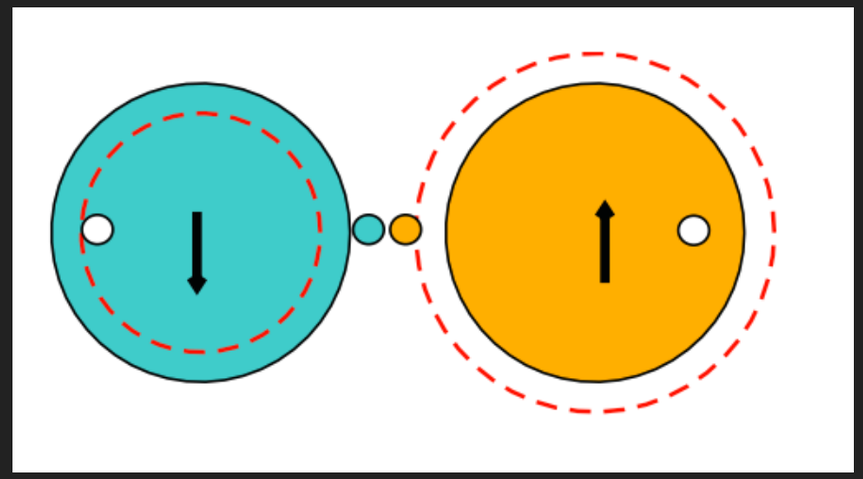

Resilient Fermi Liquid and Strength of Correlations near an Antiferromagnetic Quantum Critical Point

Phys. Rev. Lett. 128, 087001 (2022)

C. Gauvin-Ndiaye, M. Setrakian and A.-M. S. Tremblay

UNIVERSITÉ DE SHERBROOKE

INSTITUT QUANTIQUE

2D Hubbard model for e-doped cuprates

- We model the electron-doped cuprate NCCO using the **2D Hubbard model** $H = -\sum_{i,j,\sigma} t_{ij} c^{\dagger}_{i\sigma} c_{j\sigma} + U \sum_{i} n_{i\uparrow} n_{i\downarrow}$

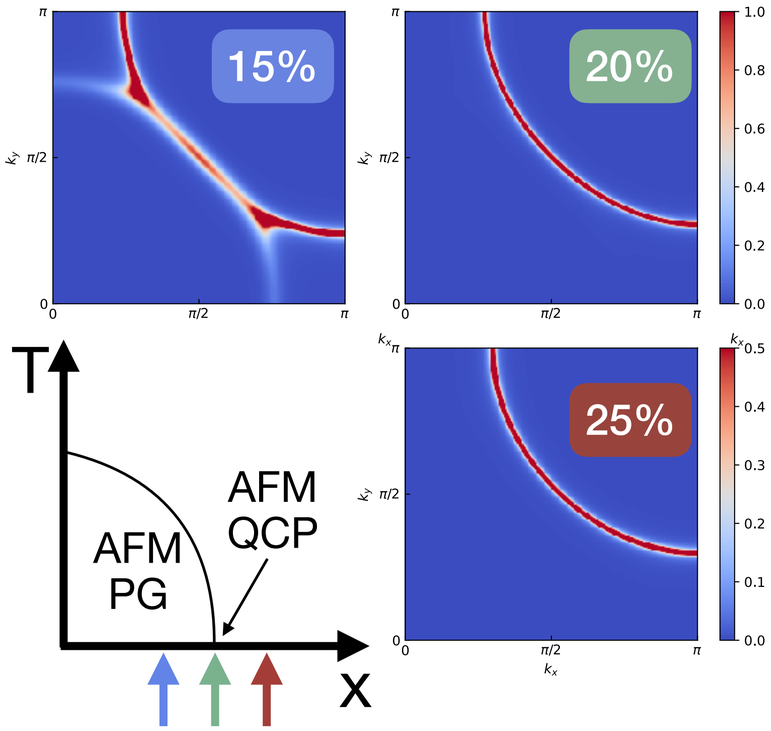

Anisotropy of the Fermi liquid quasiparticles

- The imaginary part of the self-energy of a Fermi liquid is:

$$\Sigma''(\omega, T) = a_0(T) - a_2\omega^2$$

- The Fermi liquid is also characterized by the **quasiparticle weight**:

$$Z = \left(1 - \frac{\partial \Sigma'(\omega)}{\partial \omega}\right)^{-1}\Bigg|_{\omega=0}$$

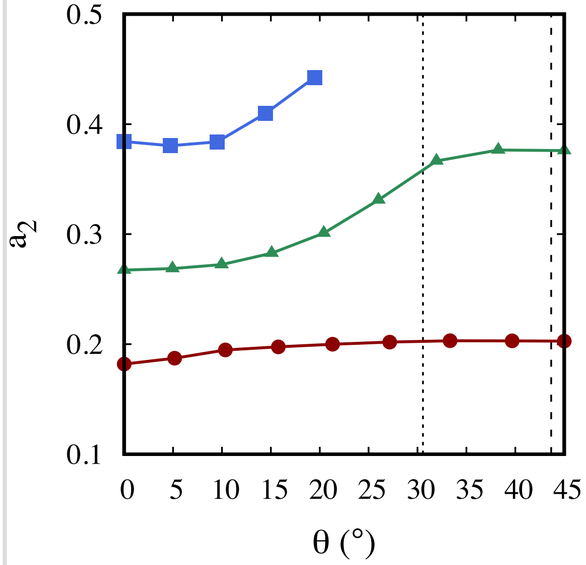

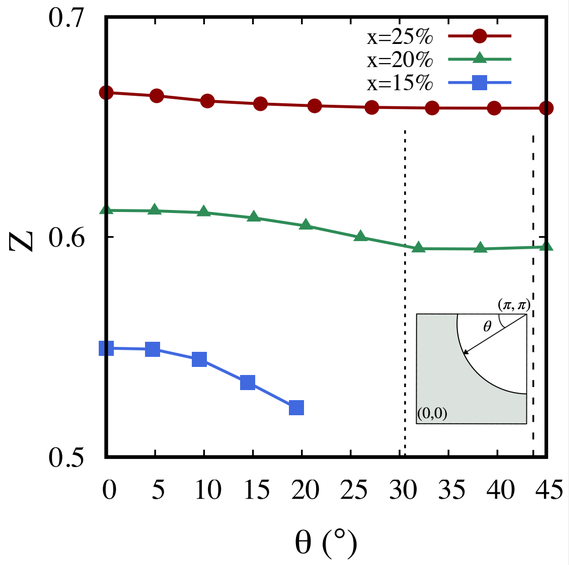

Multipolar Bose-Fermi Kondo model in Cubic Compounds

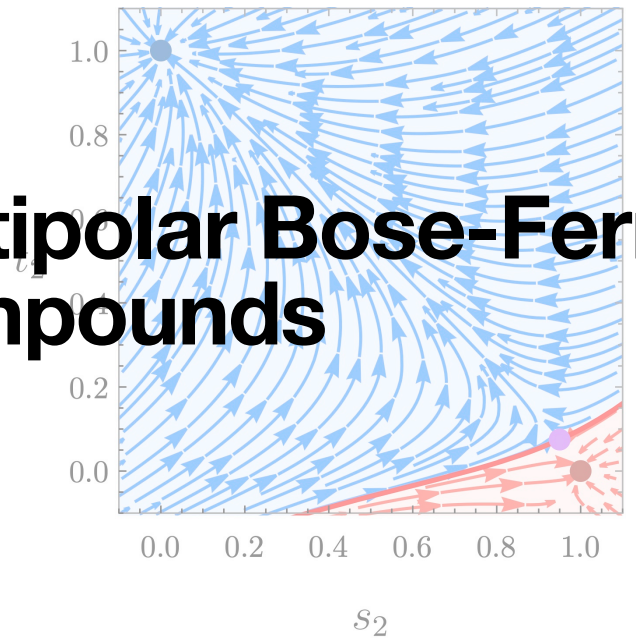

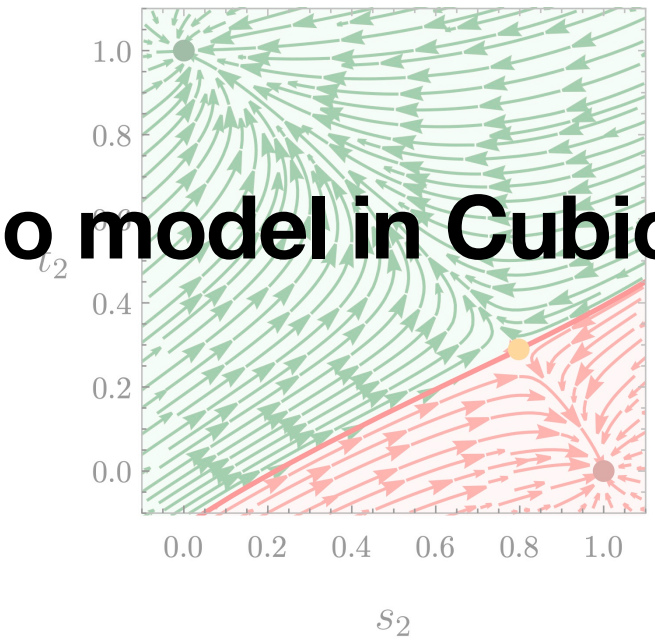

Studying transitions between non-Fermi liquids and magnetic ordering in multipolar Kondo lattices: the case of $Pr(Ti,V)_2Al_{20}$

Daniel J. Schultz, Sang Eun Han, and Yong Baek Kim
University of Toronto

Modelling Magnetic Multipolar Phases in Density Functional Theory

Dario Fiore Mosca, Leonid V. Pourovskii and Cesare Franchini

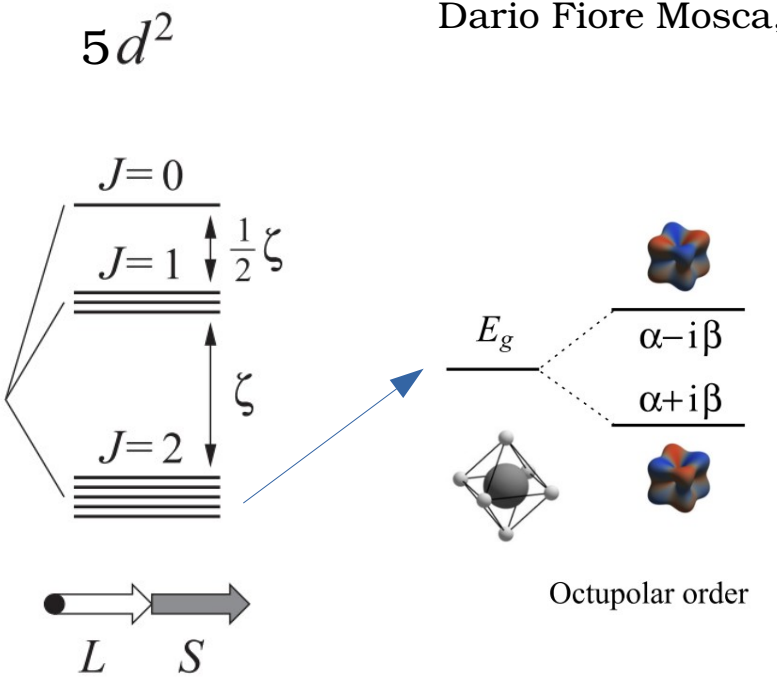

DFT + DMFT (HUB-I) + DFT

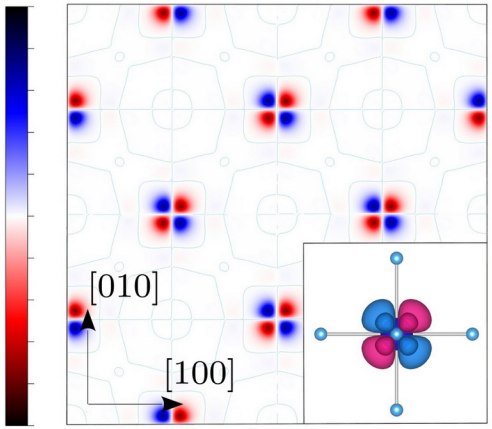

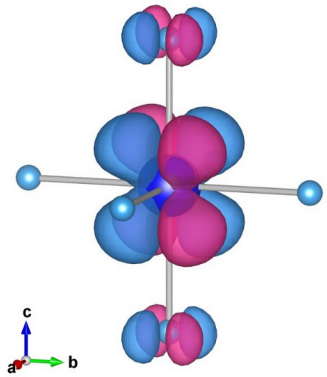

universität wien

VDS VIENNA - DOCTORAL - SCHOOL - PHYSICS

INSTITUT FRANÇAIS Autriche

Geothermal tracking of FeO's quantum critical regime: an eDMFT study

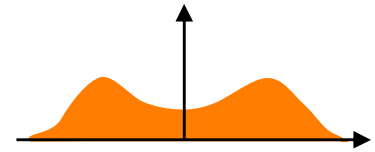

- → FeO has attracted interdisciplinary attention from both geophysical and condensed matter communities alike
- → Using Prof. Haule's embedded dynamical mean-field theory (eDMFT), we've reconstructed the phase diagram of FeO in its most geophysically relevant (B1) structural phase
- → Main findings:
  - ➢ FeO's phase diagram comprise 3 distinct regions (Mott, quantum critical, quasiparticle)
  - ➢ geophysically relevant (P, T) conditions lie mainly in the intermediate quantum critical regime – here, incoherent transport trends display:
    - weak (P, T)-dependence, in line with critical scaling behavior
    - moderate electrical resistance, approaching the Mott-Ioffe-Regel limit

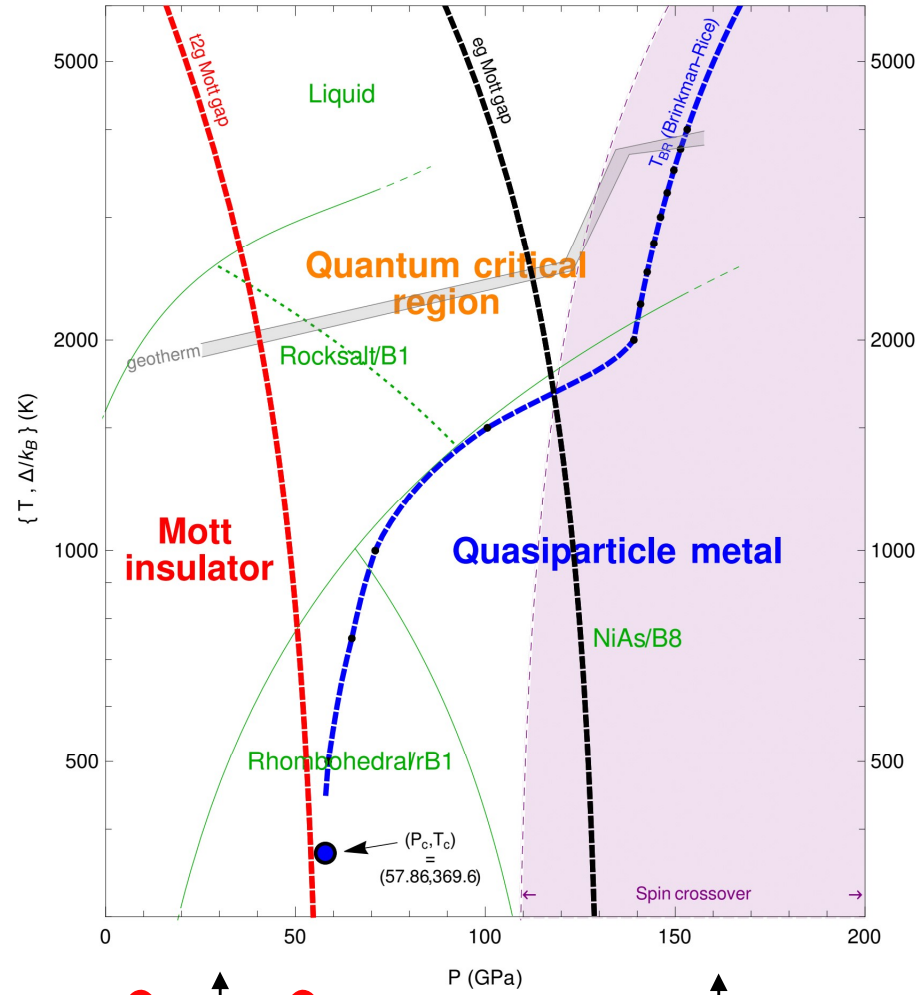

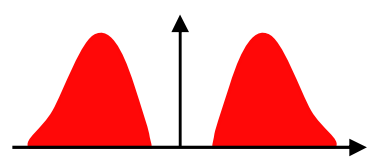

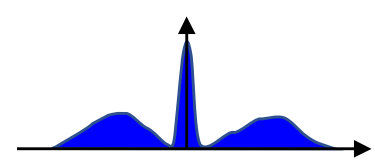

Presenter: Wai-Ga David Ho
Affiliation: NHMFL @ FSU

Int'l Summer School on Computational Quantum Materials 2022

Spin-orbit coupling and non-local correlations with the Two-Particle Self-Consistent method

Dominik Lessnich,[1] Aleksandar Razpopov,[1] Karim Zantout,[1] Steffen Backes[2] and Roser Valentí[1]

[1] Institute of Theoretical Physics, Goethe University Frankfurt, Frankfurt am Main, Germany
[2] CPHT, CNRS, Ecole Polytechnique, Institut Polytechnique de Paris, Route de Saclay, 91128 Palaiseau, France

GOETHE UNIVERSITÄT FRANKFURT AM MAIN

Spin-orbit coupling (SOC) is important to describe many materials, e.g. Sr_2RuO_4

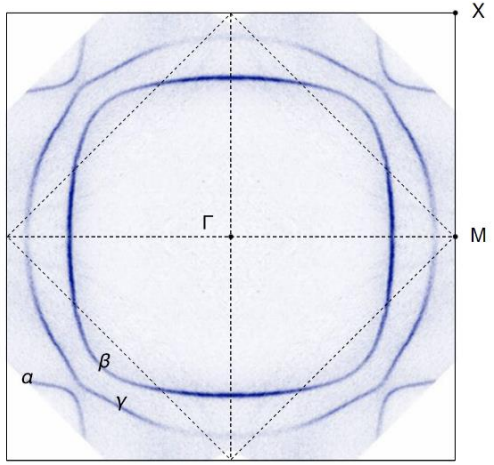

Tamai et al. Phys. Rev. X 9, 021048 (2019)

The Two-Particle Self-Consistent method (TPSC) is a many-body method able to investigate non-local correlation effects

Idea: Extend TPSC to include SOC

Problem: TPSC relies on spin rotation symmetry, which is broken when including SOC

Solution: Use time-reversal symmetry instead

Test our approach for simple model systems

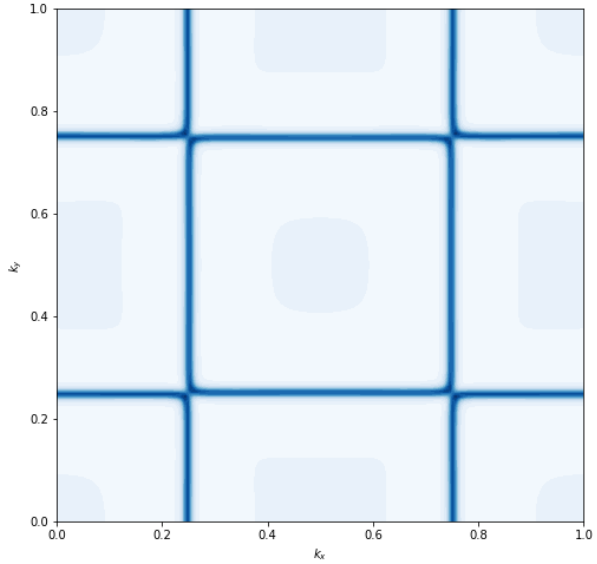

Revealing the nature of magnetic interactions by inelastic neutron scattering measurements on the honeycomb magnet $BaCo_2(AsO_4)_2$

A comprehensive inelastic neutron scattering study on the Kitaev candidate BCAO.
We examine two leading theoretical models: the Kitaev-type JKΓΓ′ model and the XXZ-J1-J3 model.

***Felix Desrochers*, *Emily Z. Zhang*,**
Thomas Halloran, Collin Broholm, Yong Baek Kim

UNIVERSITY OF TORONTO

Revealing the nature of magnetic interactions by inelastic neutron scattering measurements on the honeycomb magnet $BaCo_2(AsO_4)_2$

A comprehensive inelastic neutron scattering study on the Kitaev candidate BCAO.
We examine two leading theoretical models: the Kitaev-type JKΓΓ′ model and the XXZ-J1-J3 model.

***Felix Desrochers*, *Emily Z. Zhang*,**
Thomas Halloran, Collin Broholm, Yong Baek Kim

UNIVERSITY OF TORONTO

Cavity Perturbation Theory

Fabian Künzel
Friedrich-Alexander-Universität Erlangen-Nürnberg

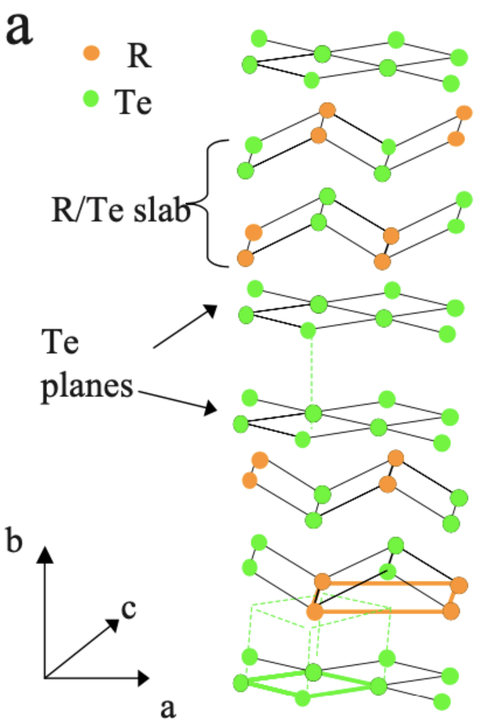

Brouet, V. et al. (2008). Angle-resolved photoemission study of the evolution of band structure and charge density wave properties in RTe_ {3}(R= Y, La, Ce, Sm, Gd, Tb, and Dy).

Charge-Density-Wave susceptibility

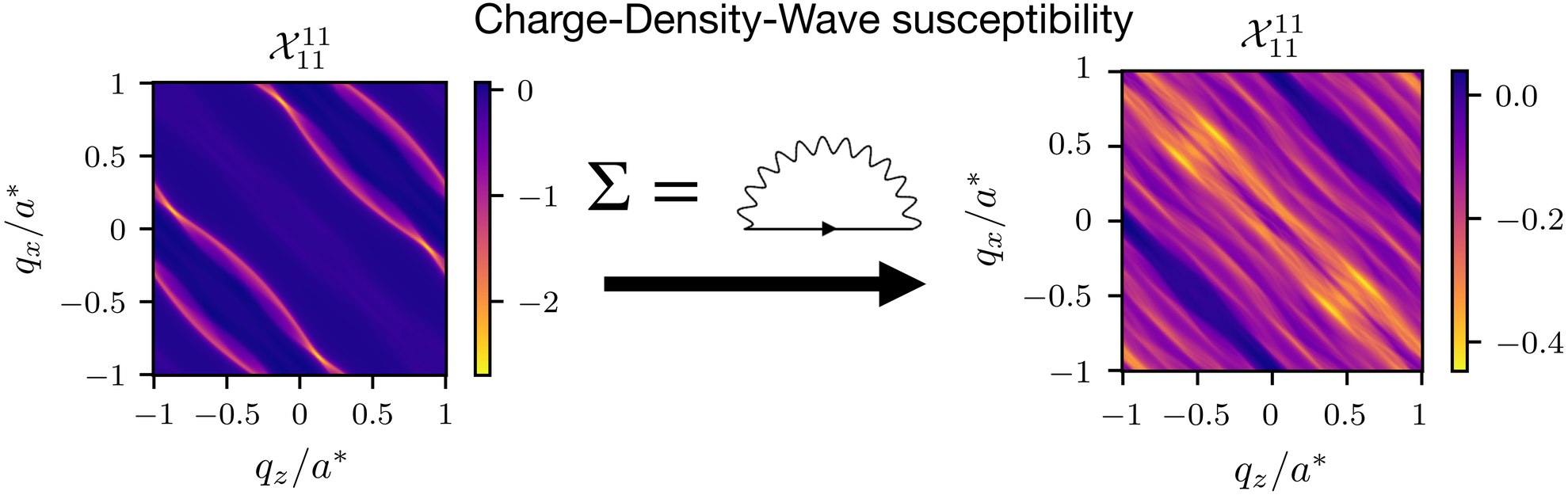

Change in Charge-Density-Wave phase transition?

Multiconfigurational approach to XAS and XMCD for Co- and Ni- doped magnetite

Felix Sorgenfrei
Uppsala University

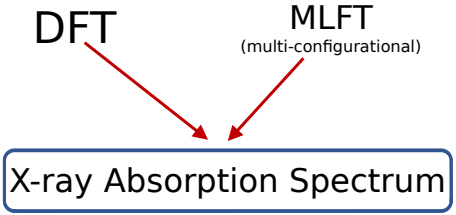

MLFT: Multiplet Ligand Field Theory

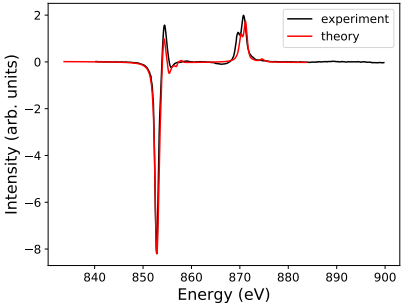

Figure: Calculated Ni $L_{2,3}$ edge XMCD in $NiFe_2O_4$

UPPSALA UNIVERSITET

A DMFT look on the magnetic ground state of Ba_2YIrO_6

5d^4 double perovskite, strong SOC and correlations

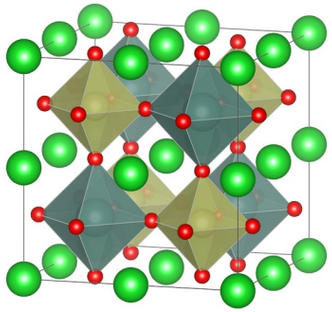

Exotic Magnetism

- Atomic picture J=0, in experiment finite moment

DFT+DMFT calculations

- At finite and zero temperature using QMC & DMRG based impurity solvers
- Finite moment due to hopping
- **BUT:** Dynamic correlations destroy long-range ordering

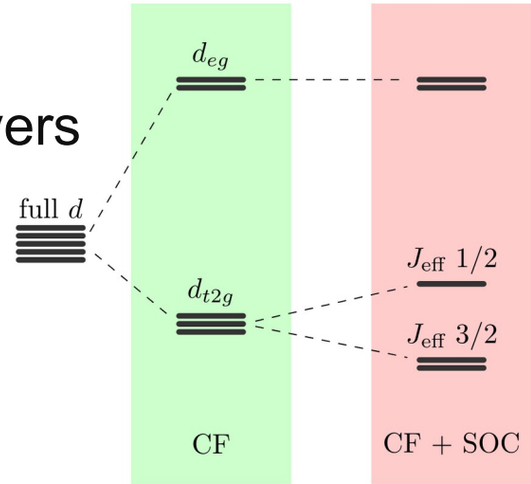

Hermann Schnait
Technical University Graz, Austria

arXiv:2202.10794

How the Hund's correlations respond to electronic structures of multiorbital systems

Hyeong Jun Lee
Korea Advanced Institute of Science and Technology (KAIST), Korea

Korea Advanced Institute of Science and Technology

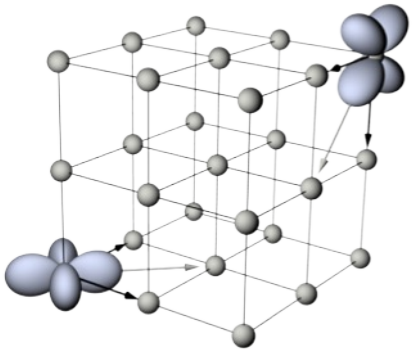

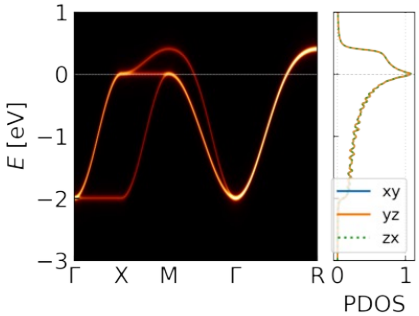

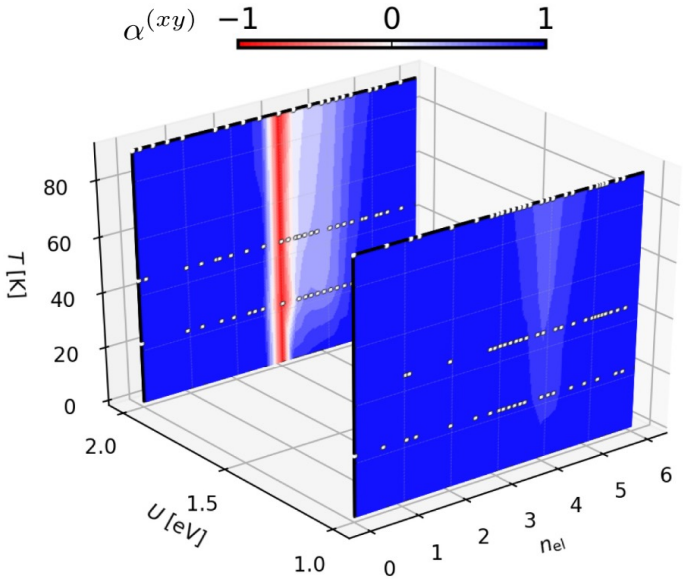

- Hund's metallicity
  - Effects of vHS
  - Orbital characters
- Three t_{2g} bands model
- DMFT-ED reaching T=0

HJL, Choong H. Kim, Ara Go, *Phys. Rev. B* **104**, 165138 (2021).

Strategy to Extract Kitaev Interaction using Symmetry in Honeycomb Mott Insulators

Jiefu Cen and Hae-Young Kee

Department of Physics, University of Toronto

International Summer School on Computational Quantum Material

- Lack of C_{2a} symmetry in honeycombs of edge-sharing octahedra and the $JK\Gamma\Gamma'$ spin Hamiltonian

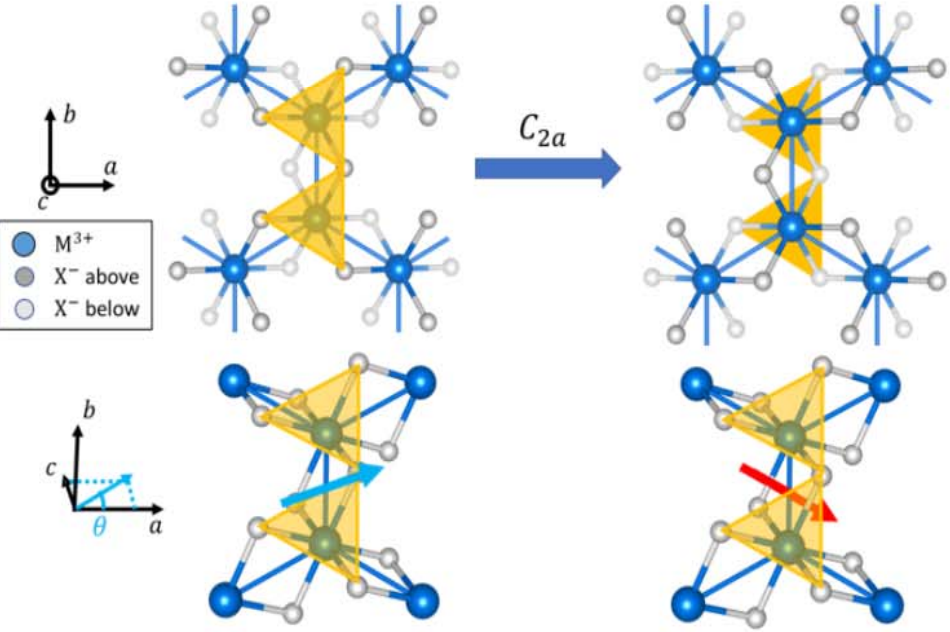

- Lack of C_{2a} due to $J_{ac} \propto K - \Gamma$ and use of magnetic field to detect it

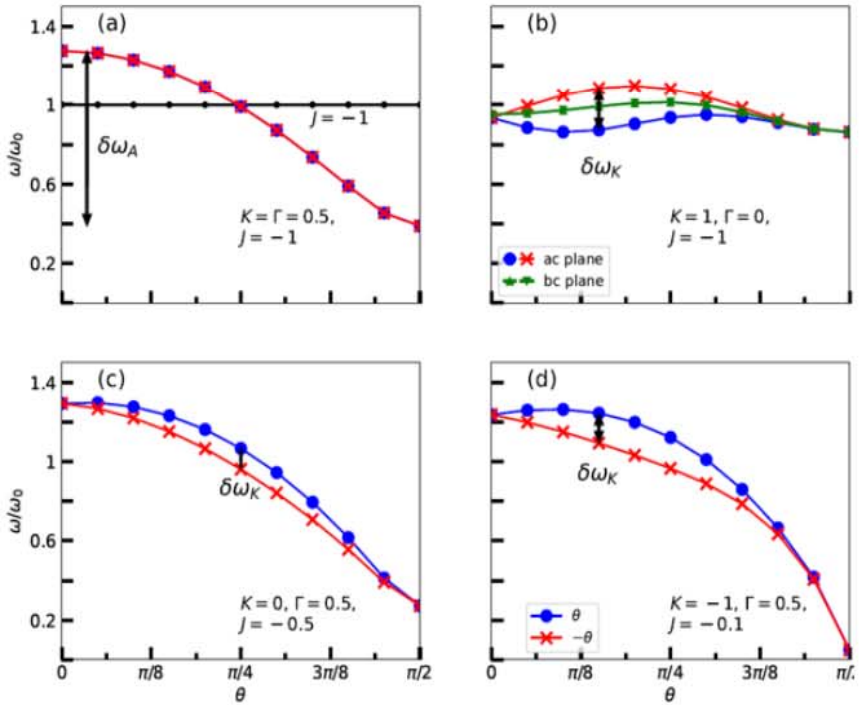

Cen, J., Kee, HY. *Commun Phys* **5,** 119 (2022).

Information-theoretic measures of superconductivity in a two-dimensional doped Mott insulator

Caitlin Walsh (Department of Physics, Royal Holloway University of London, UK)

- Entanglement-based tools from quantum information theory can describe various phases of interacting quantum systems on a lattice
- Entanglement perspective complements thermodynamic descriptions
- Our contribution: Local entropy and mutual information can detect and describe superconductivity!
- We find upon doping a Mott insulator that the local entropy reflects the source of the condensation energy and the mutual information is amplified in the superconducting state

$$s_1 = -\sum_i p_i \ln(p_i)$$

$$\overline{I_1} = s_1 - s$$

C. Walsh, M. Charlebois, P. Sémon, G. Sordi, and A.-M.S. Tremblay

Proc. Natl. Acad. Sci. 10.1073/pnas.2104114118 (2021)

ROYAL HOLLOWAY UNIVERSITY OF LONDON

UQTR Université du Québec à Trois-Rivières

Brookhaven National Laboratory

UNIVERSITÉ DE SHERBROOKE

compute canada

Higher angular momentum pairings in interorbital superconductors

Jonathan Clepkens[1], Austin W. Lindquist[1], Xiaoyu Liu[1], and Hae-Young Kee[1,2]

(1) Department of Physics, University of Toronto, 60 St. George St., Toronto, Ontario, M5S 1A7, Canada (2) Canadian Institute for Advanced Research, Toronto, Ontario, M5G 1Z8, Canada

$$\hat{\mathbf{d}}_{a/b} = \frac{1}{4N}\sum_{\mathbf{k}\sigma\sigma'}[i\sigma^y\boldsymbol{\sigma}]_{\sigma\sigma'}\left(c^a_{\mathbf{k}\sigma}c^b_{-\mathbf{k}\sigma'} - c^b_{\mathbf{k}\sigma}c^a_{-\mathbf{k}\sigma'}\right)$$

$$i\Delta_{\mathbf{k}}\left[\left(c_{\beta,\mathbf{k}+}c_{\beta,-\mathbf{k}-} - c_{\beta,\mathbf{k}-}c_{\beta,-\mathbf{k}+}\right) - \left(c_{\gamma,\mathbf{k}+}c_{\gamma,-\mathbf{k}-} - c_{\gamma,\mathbf{k}-}c_{\gamma,-\mathbf{k}+}\right)\right] + \text{H.c.}$$

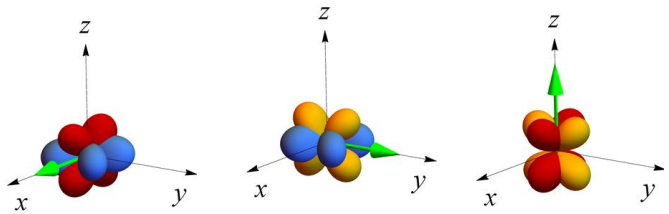

$d^x_{xz/xy}$ $d^y_{xy/yz}$ $d^z_{yz/xz}$

d- and g-wave interorbital pairing

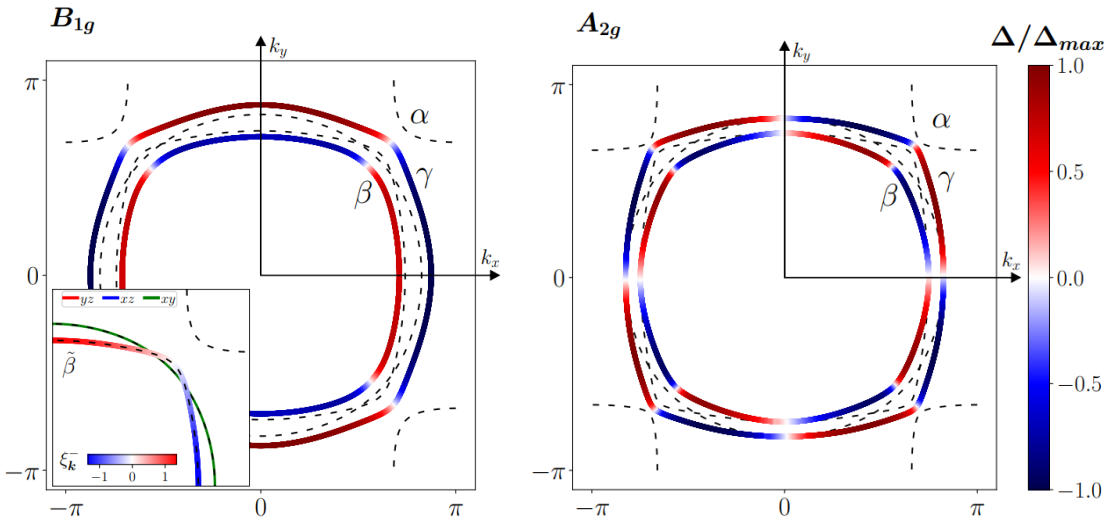

$$\Delta_{\mathbf{k}} \sim \frac{|d^x_{xz/xy}|}{E_{1d,\mathbf{k}}}\lambda\,\xi^-_{\mathbf{k}} \qquad \sim \frac{|d^y_{xz/xy}|}{E_{1d,\mathbf{k}}}\lambda_{B_{2g}}\sin k_x \sin k_y\,\xi^-_{\mathbf{k}}$$

Application to Sr_2RuO_4

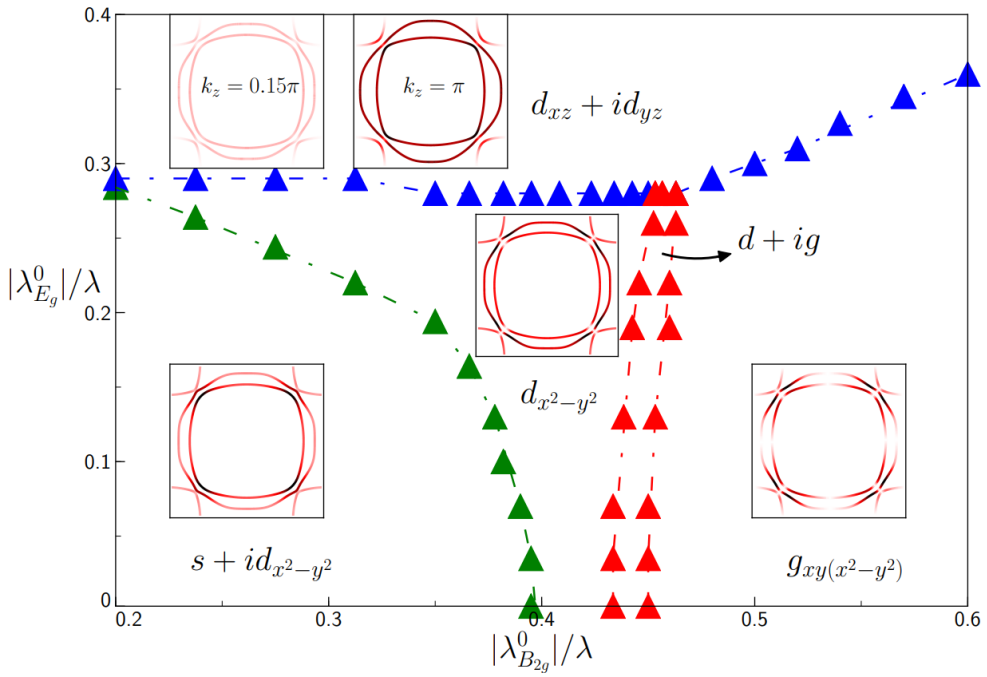

J. Clepkens, A.W. Lindquist, X. Liu, and H.-Y. Kee PRB 104, 104512 (2021); J. Clepkens, A.W. Lindquist, and H.-Y. Kee PRR 3, 013001 (2021)

UNIVERSITY OF TORONTO SciNet

Spin-Orbital polaron in a $5d^1$ Osmate

Lorenzo Celiberti, Dario Fiore Mosca, Cesare Franchini

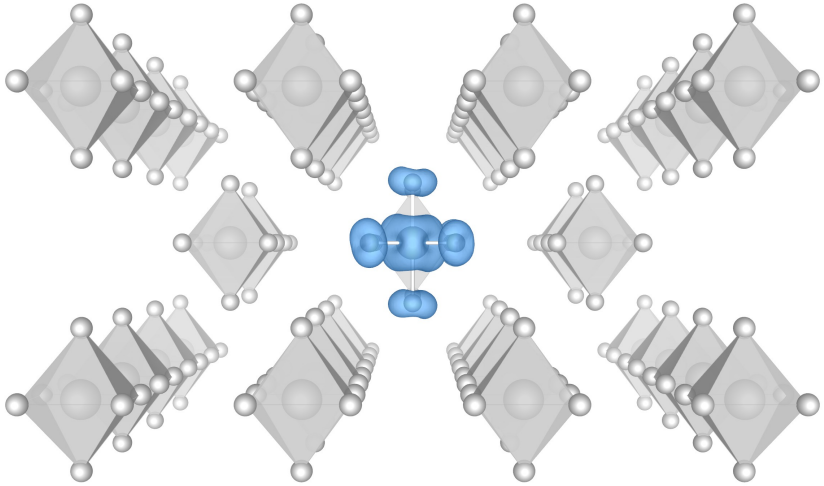

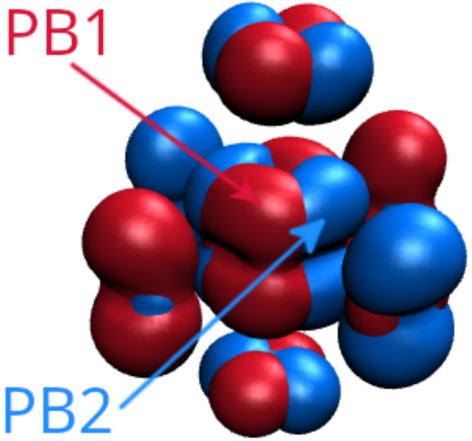

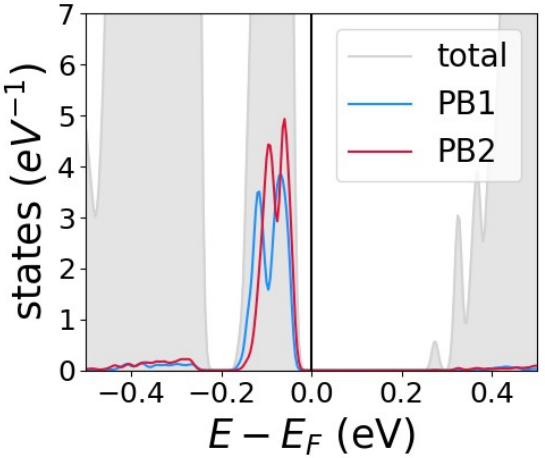

universität wien

b-initio ackage imulation ienna

VIENNA SCIENTIFIC CLUSTER

AB INITIO STUDY OF RARE-EARTH NICKELATES THROUGH ADVANCED HUBBARD FUNCTIONALS

Luca Binci, Michele Kotiuga, Iurii Timrov and Nicola Marzari

THEOS and NCCR-MARVEL, École Polytechnique Fédérale de Lausanne (EPFL), Lausanne, Switzerland

International Summer School on Computational Quantum Materials - June 2022

Theoretical method: DFT+U+V

$$E_{\mathrm{DFT}+U+V} = E_{\mathrm{DFT}} + \sum_I \frac{U^I}{2} \sum_{m,\sigma} \left[n^{II\sigma}_{mm} - \sum_{m'} n^{II\sigma}_{mm'} n^{II\sigma}_{m'm} \right] - \sum_{\langle I,I' \rangle} \frac{V^{II'}}{2} \sum_{\{m\},\sigma} n^{II'\sigma}_{mm'} n^{I'I\sigma}_{m'm}$$

On-site (localisation)

Inter-site (hybridisation)

Rare-earth nickelates - RNiO$_3$

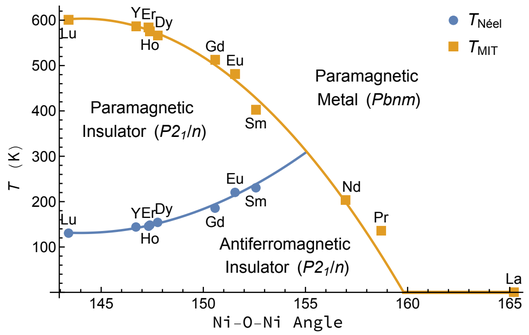

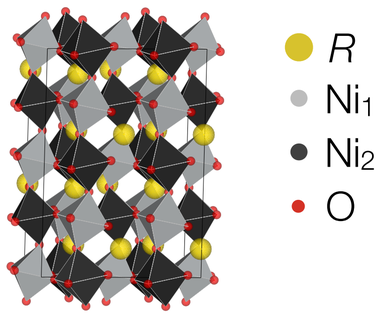

Investigated magnetic orderings

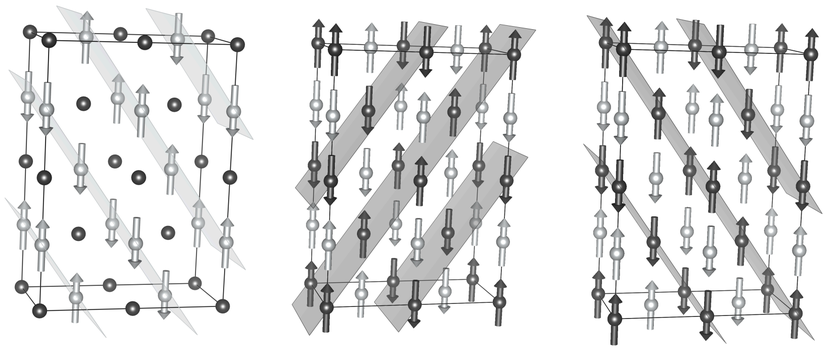

B-type *S*-type *T*-type

Main results

- According to out model, purely **on-site** contribution are **not enough** to obtain a physical picture compliant with experiments.
- The **inter-site** term is necessary to obtain at self-consistency the structural **disproportionation**, the stabilisation of the correct **AFM** order and the **insulating** state.
- We predict the materials to be **multiferroic**, in accordance with recent experimental observations.

SUBGAP STATES IN SUPERCONDUCTORS WITH CHARGING ENERGY

Luka Pavešič, Rok Žitko, Jožef Stefan Institute and University of Ljubljana, Slovenia

Jožef Stefan Institute

University of Ljubljana

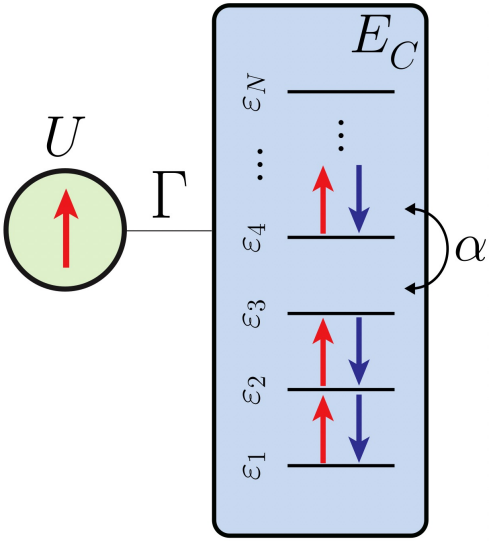

We use a *charge conserving* model of superconductivity to describe small superconducting islands coupled to quantum dots.

Charging energy produces *qualitative differences* in subgap spectra, which are in *great agreement with experiment*.

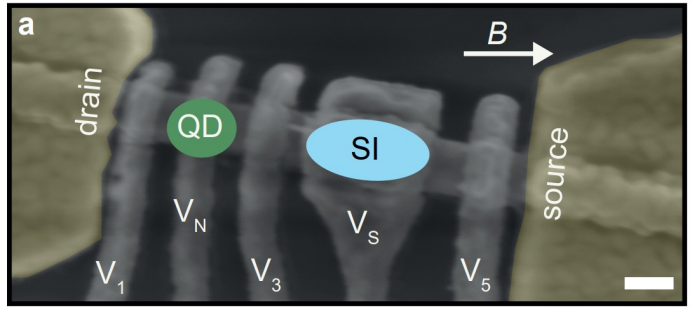

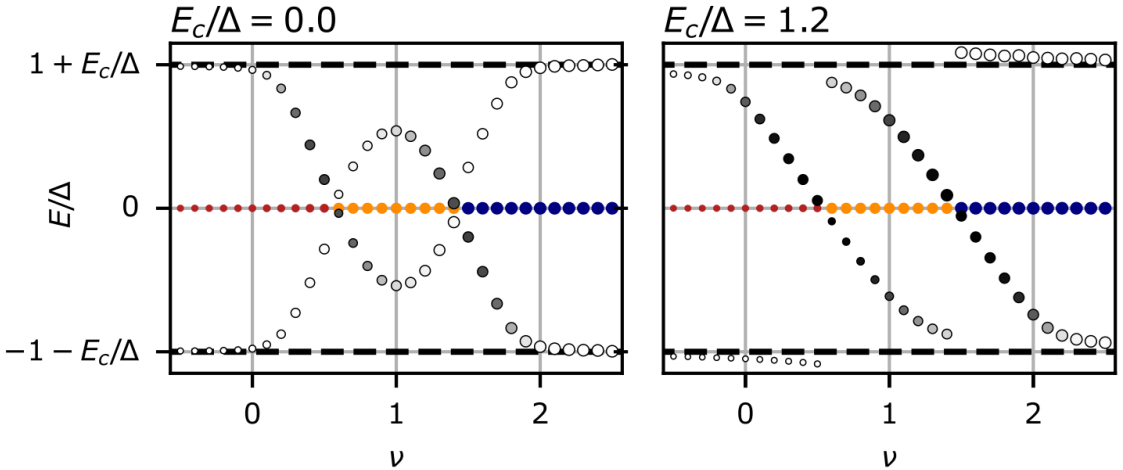

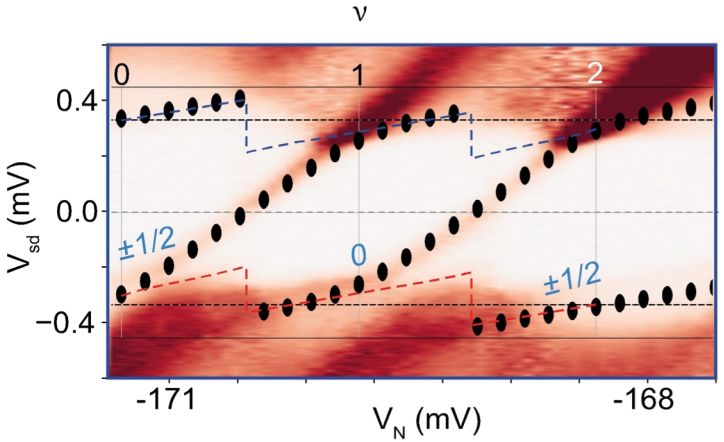

Engineering Helical Edge Modes in Stanene with Adatoms

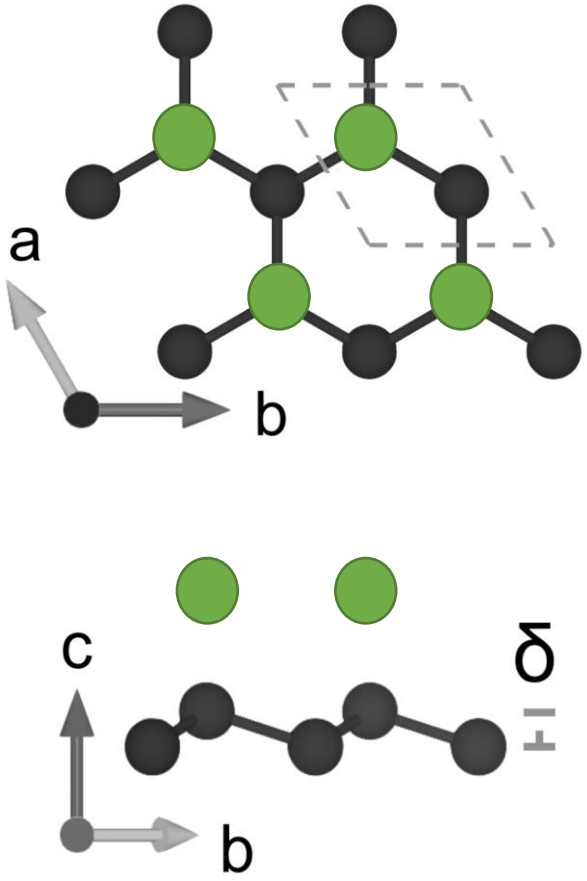

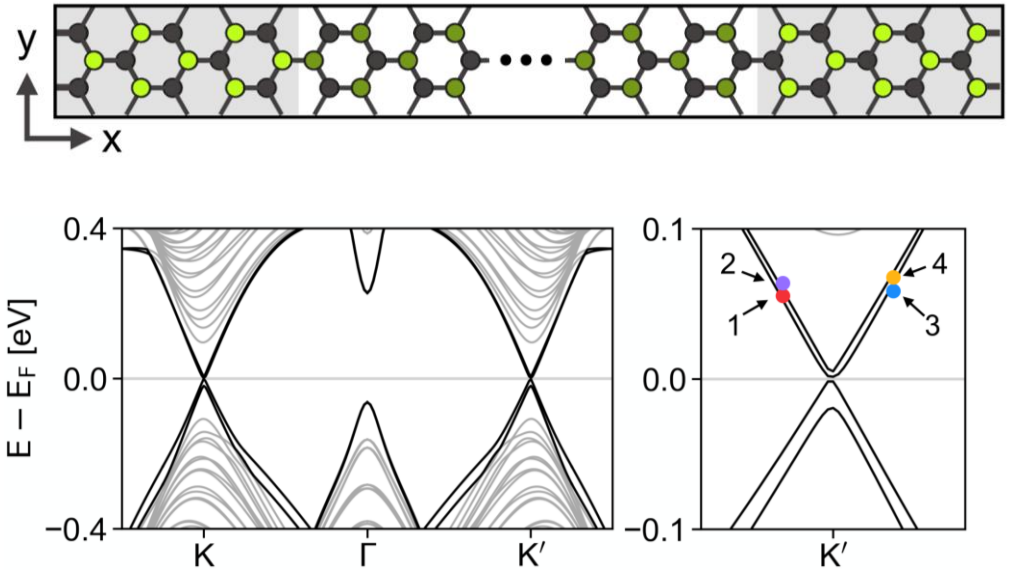

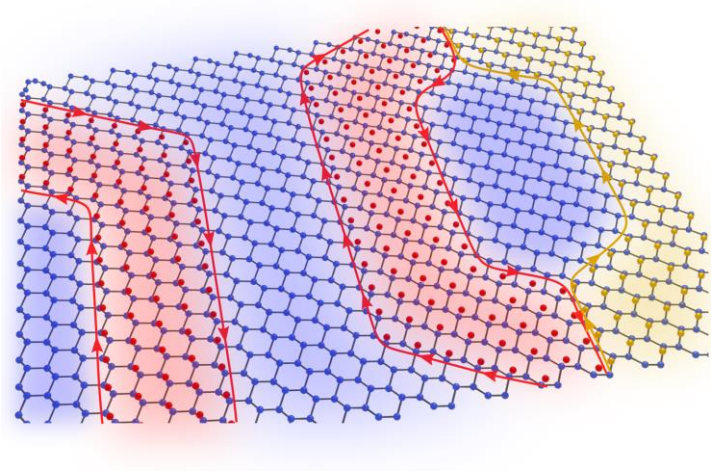

Mark Hirsbrunner

Collaborators: Jenny Coulter, Oleg Dubinkin, Taylor Hughes, Boris Kozinsky

U.S. DEPARTMENT OF ENERGY | Office of Science

UNIVERSITY OF ILLINOIS URBANA-CHAMPAIGN

Signatures of bosonic excitations in high-harmonic spectra of Mott insulators

Markus Lysne
University of Fribourg, Switzerland

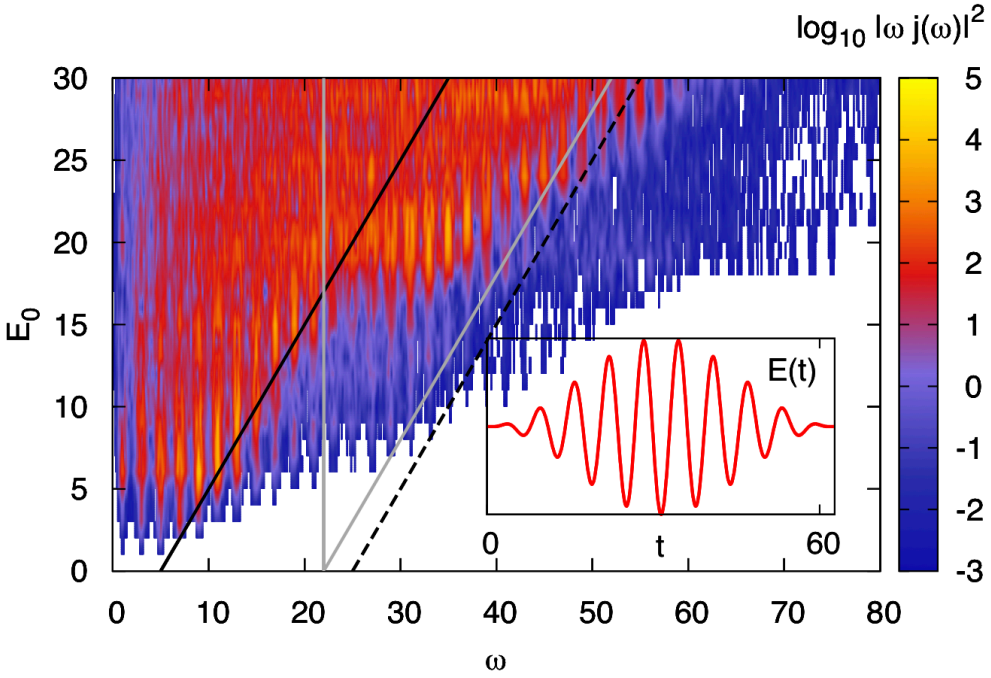

- High harmonic generation studied through non-equilibrium DMFT
- A spectroscopic tool for
  - Hubbard-Holstein model
  - Two-orbital Hubbard model with Hund coupling

Perturbation theory breakdown in correlated antiferromagnets

Matthias Reitner

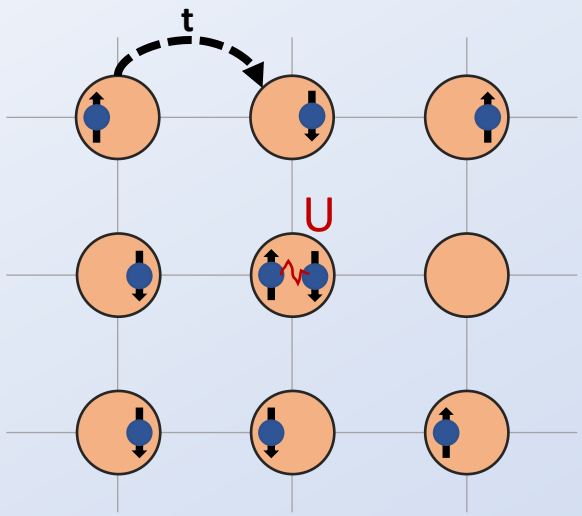

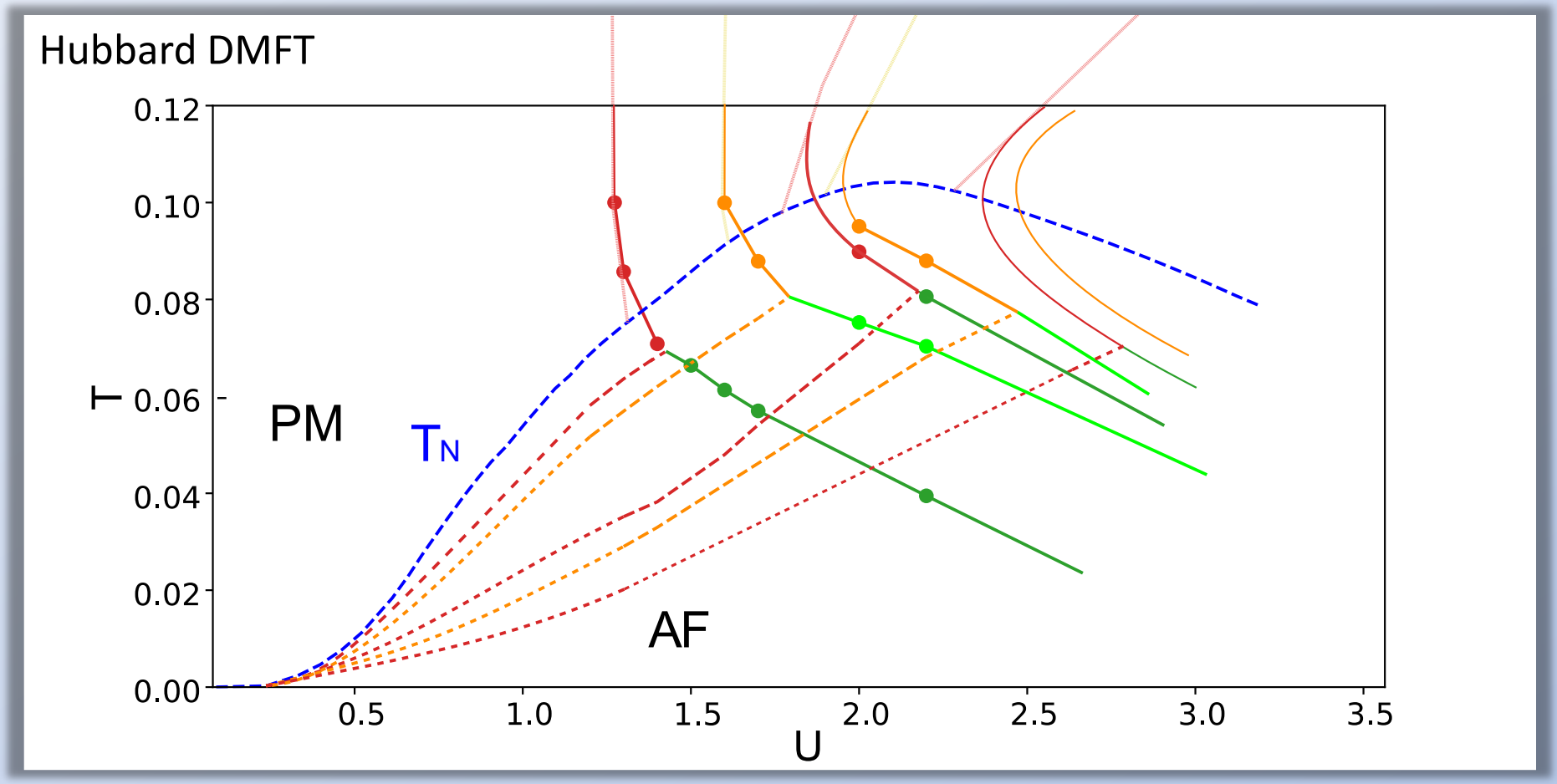

Cellular dynamical mean field theory for the Hubbard model on large real space clusters

[Michael Meixner, Group of Dr. Thomas Schäfer]
[Max Planck Institute for Solid State Research, Stuttgart; m.meixner@fkf.mpg.de]

Site resolved spectral weight

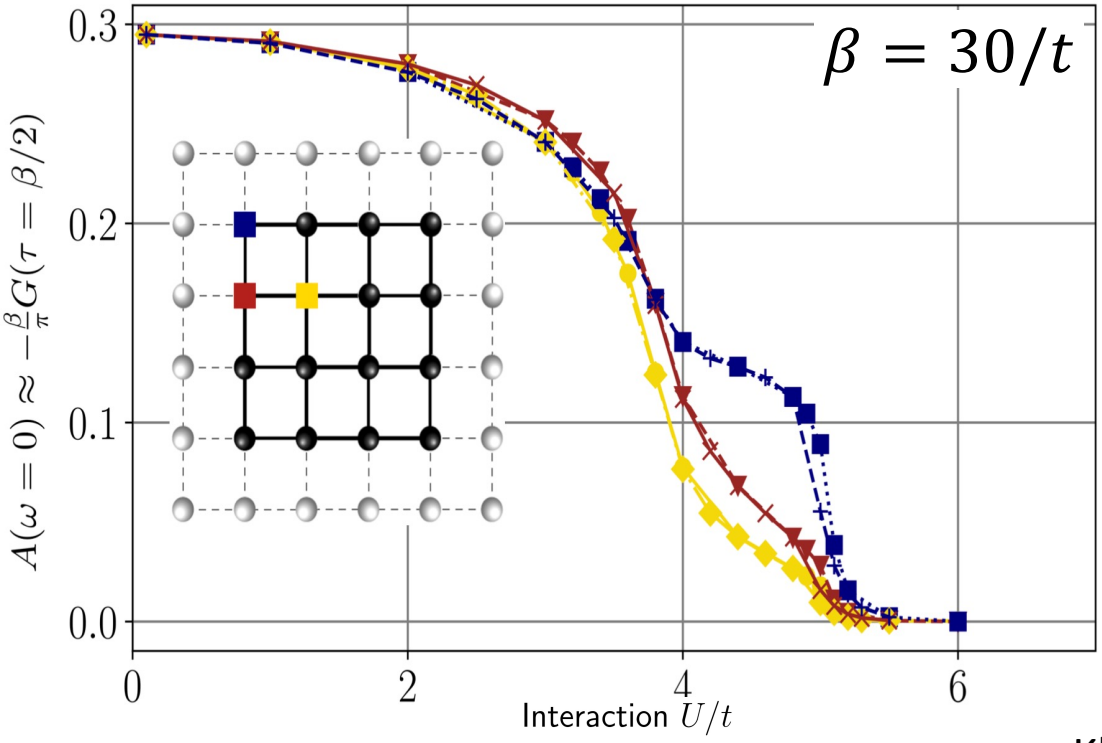

k resolved spectral weight

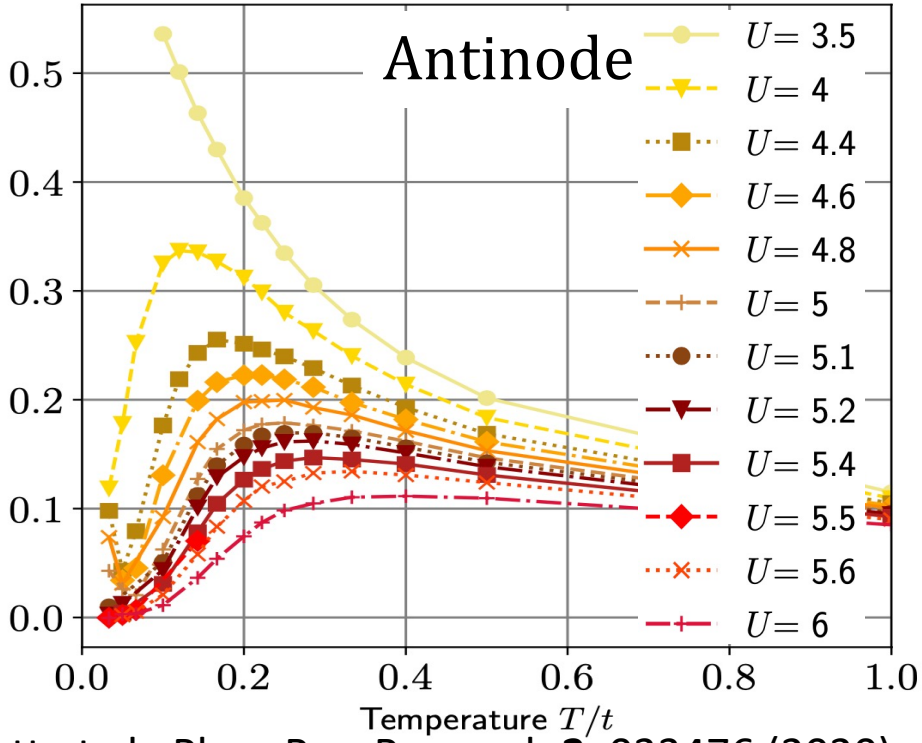

Fermi surface $A(k,\omega)$, doped

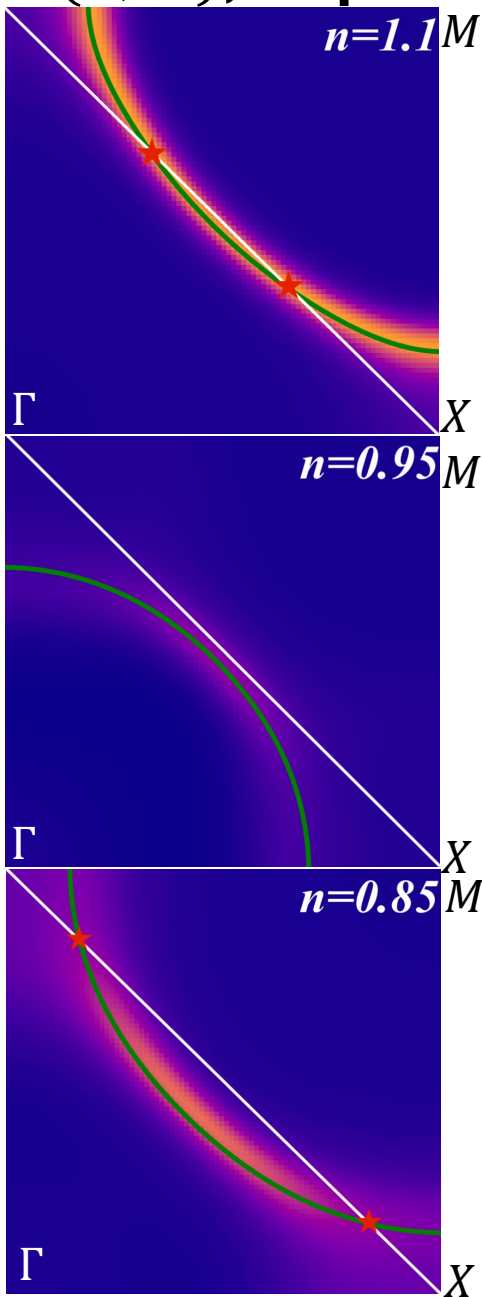

Klett et al. Phys. Rev. Research **2**, 033476 (2020)

Suppression of Peierls-like, nesting-based instabilities in solids

Nassim Derriche, Ilya Elfimov, George Sawatzky

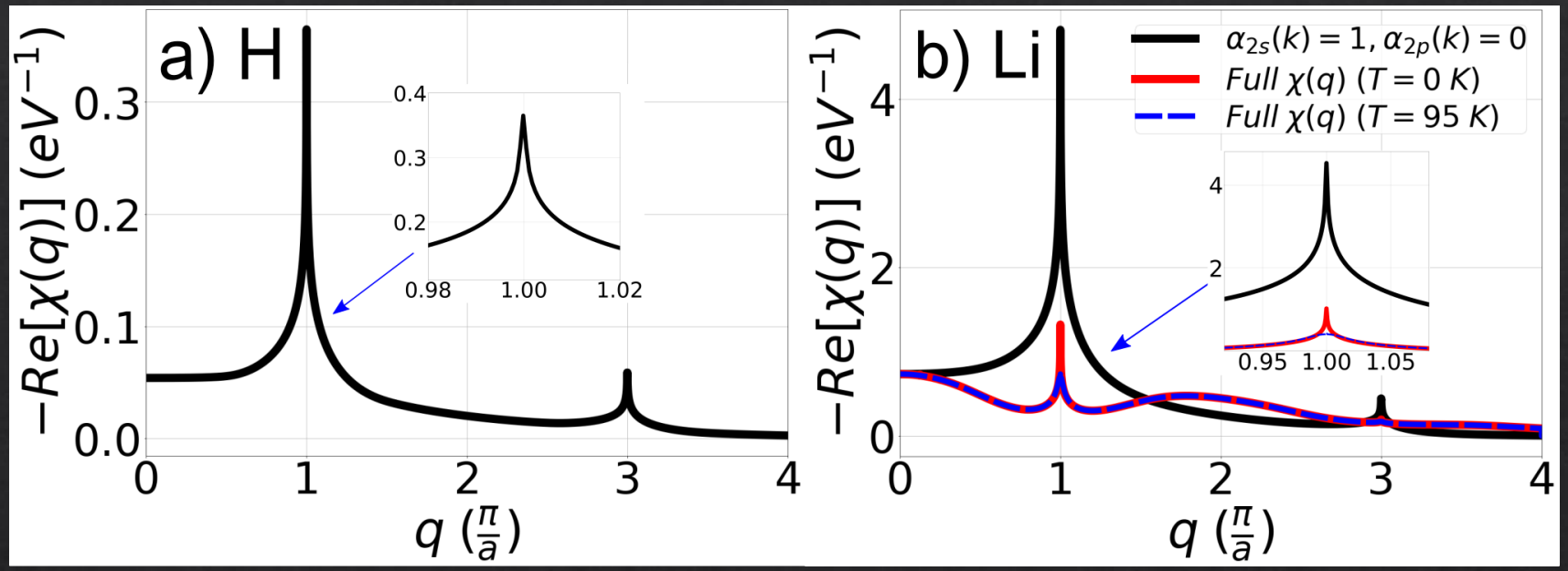

- The Peierls instability in one-dimensional chains of Lithium is quelled (as opposed to the Hydrogen chain) due to the *gerade-ungerade* mixing of the 2s and 2p orbitals, as shown by the suppression of the associated Lindhard function peak.

- Looking at nesting wavevectors is not enough for qualitative predictions of instabilities in systems for which the wavefunctions are strongly non-free electron-like, even at higher dimensions. The symmetry and parity of the charge carrier states are critical.

Keldysh mfRG Calculations for the Single Impurity Anderson Model

Elias Walter, Anxiang Ge, Nepomuk Ritz, Fabian B. Kugler and Jan von Delft

Physics Department, Arnold Sommerfeld Center for Theoretical Physics, and Center for NanoScience,
Ludwig-Maximilians-Universität, Theresienstrasse 37, 80333 Munich, Germany

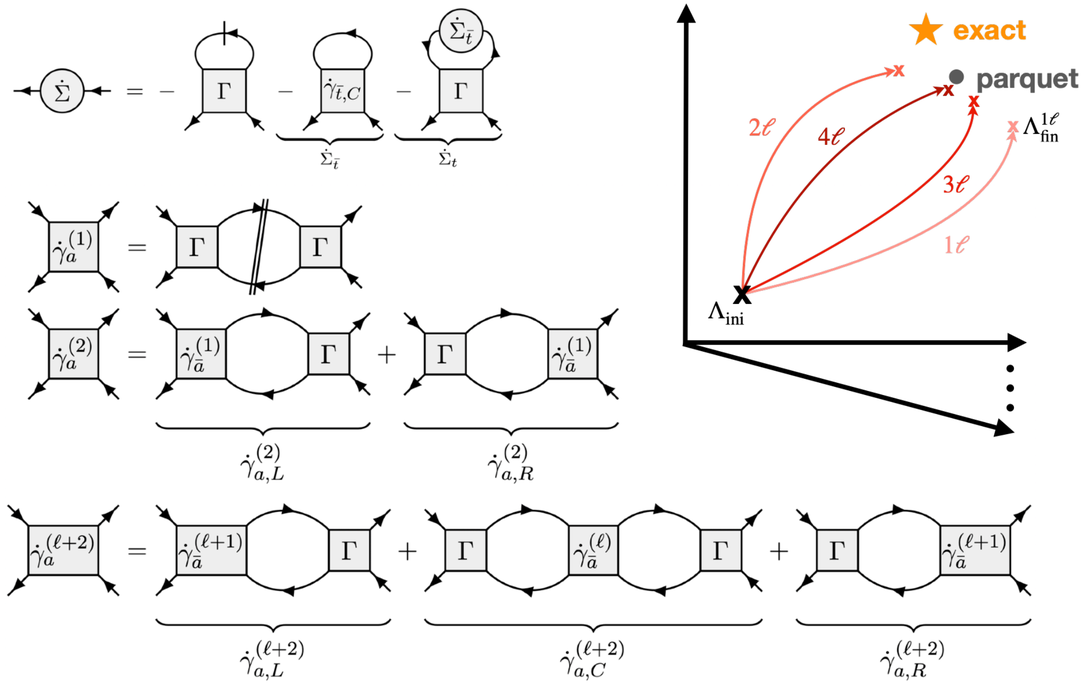

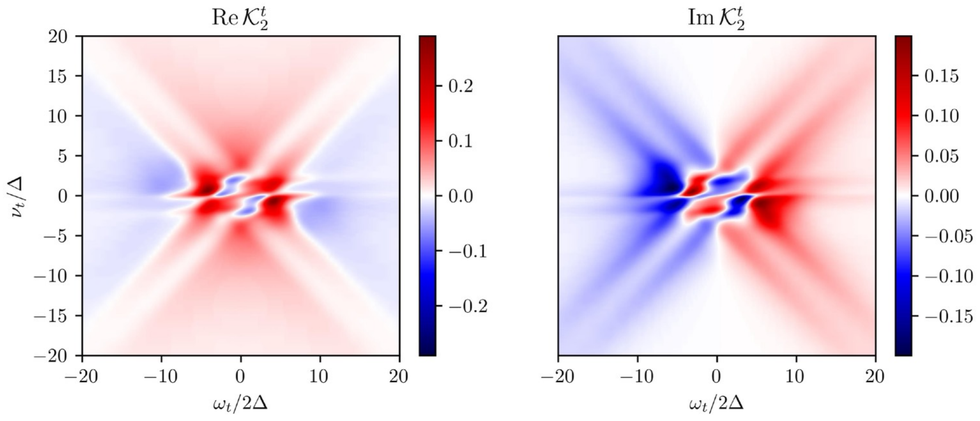

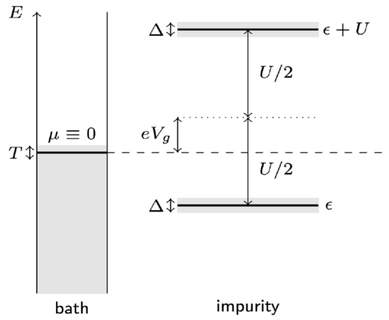

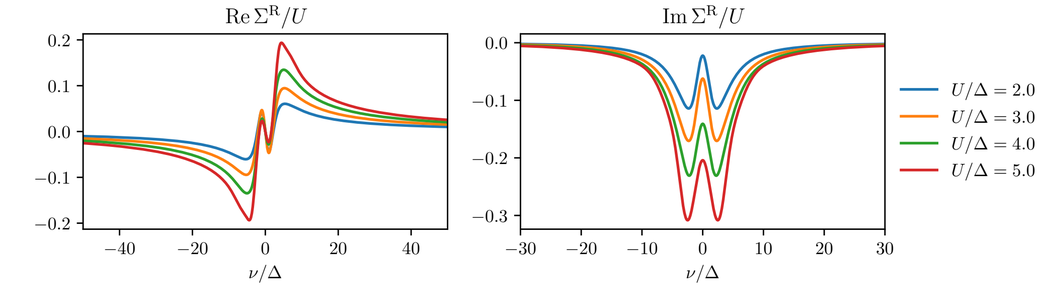

$$H = \underbrace{\sum_{m,k,\sigma} \epsilon(k)\, c^\dagger_{m,k,\sigma} c_{m,k,\sigma}}_{H_{\rm bath}} + \underbrace{\sum_\sigma \epsilon_\sigma d^\dagger_\sigma d_\sigma + U d^\dagger_\uparrow d_\uparrow d^\dagger_\downarrow d_\downarrow}_{H_{\rm imp}} + \underbrace{\sum_{m,k,\sigma} \left(t_m d^\dagger_\sigma c_{m,k,\sigma} + \mathrm{h.c.}\right)}_{H_{\rm hyb}}$$





LMU Ludwig-Maximilians-Universität München
MCQST
Studienstiftung des deutschen Volkes

Benchmark of the TPSC+DMFT approach to the Hubbard model

Nicolas Martin, Chloé Gauvin-Ndiaye, André-Marie Tremblay.
Département de Physique, RQMP and Institut Quantique, Université de Sherbrooke, Québec, Canada, J1K2R1

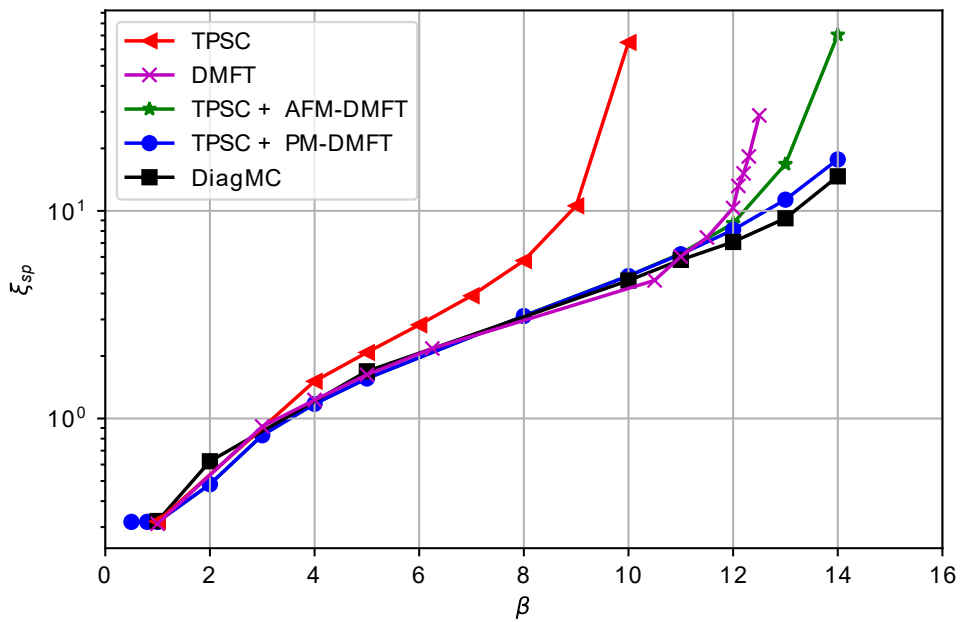

UNIVERSITÉ DE SHERBROOKE

USHERBROOKE.CA/IQ

Efficient approach to correlations and superconductivity in complex materials

Niklas Witt, I. Institute for Theoretical Physics, University of Hamburg

Problem

Complexity of real materials

Multiple energy scales and ...

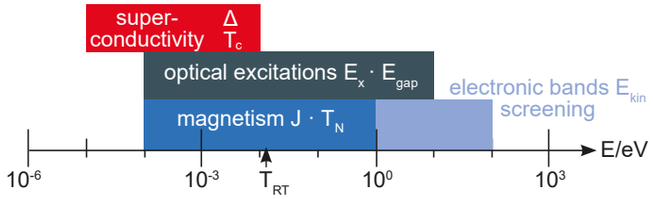

... many degrees of freedom

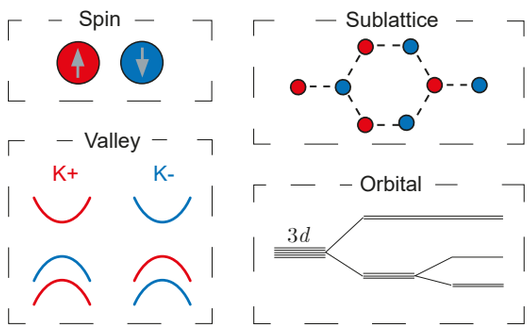

- Low T calculations demanding
- **Bottleneck** for (diagrammatic) many-body methods

Solution

Sparse sampling approach

- intermediate representation basis expansion

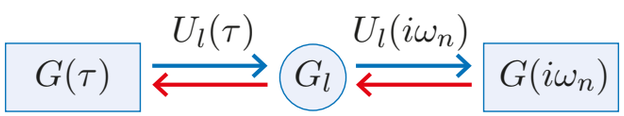

Properties:

- Controlled error
- High compactness
- Sparse grid sampling

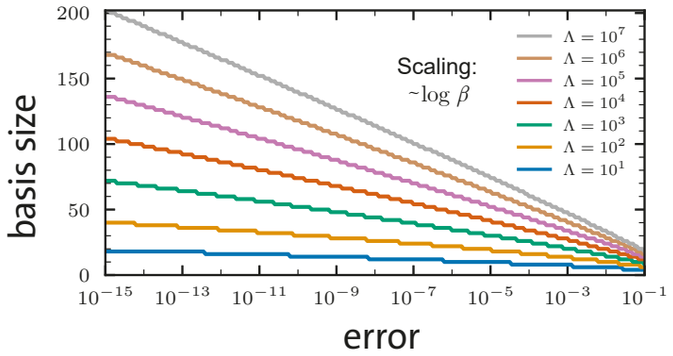

Application

$Na_xCoO_2 \cdot yH_2O$

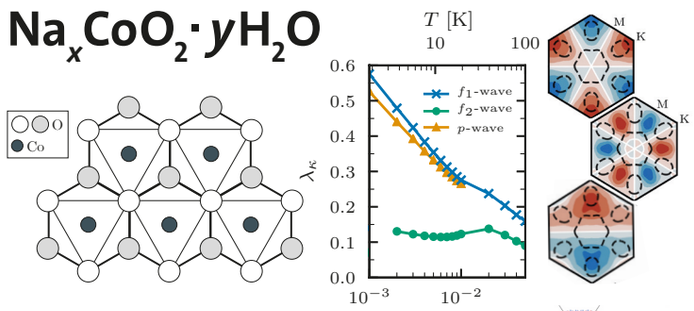

Twisted TMDCs

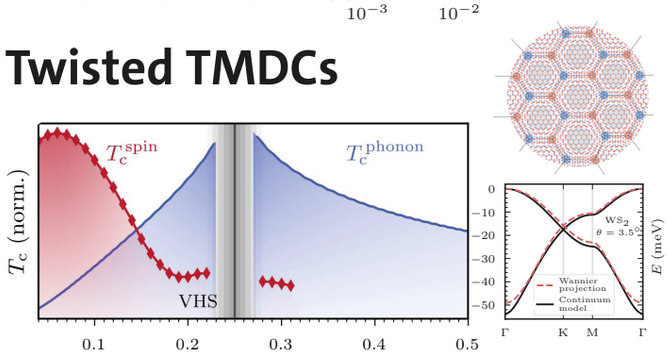

Transport in doped cuprates

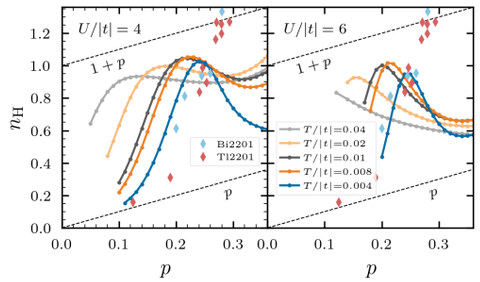

NONEQUILIBRIUM TWO-PARTICLE SELF-CONSISTENT APPROACH

Olivier Simard

Université de Fribourg

Nickelate superconductors from a DMFT + DGA perspective

TECHNISCHE UNIVERSITÄT WIEN

Paul Worm

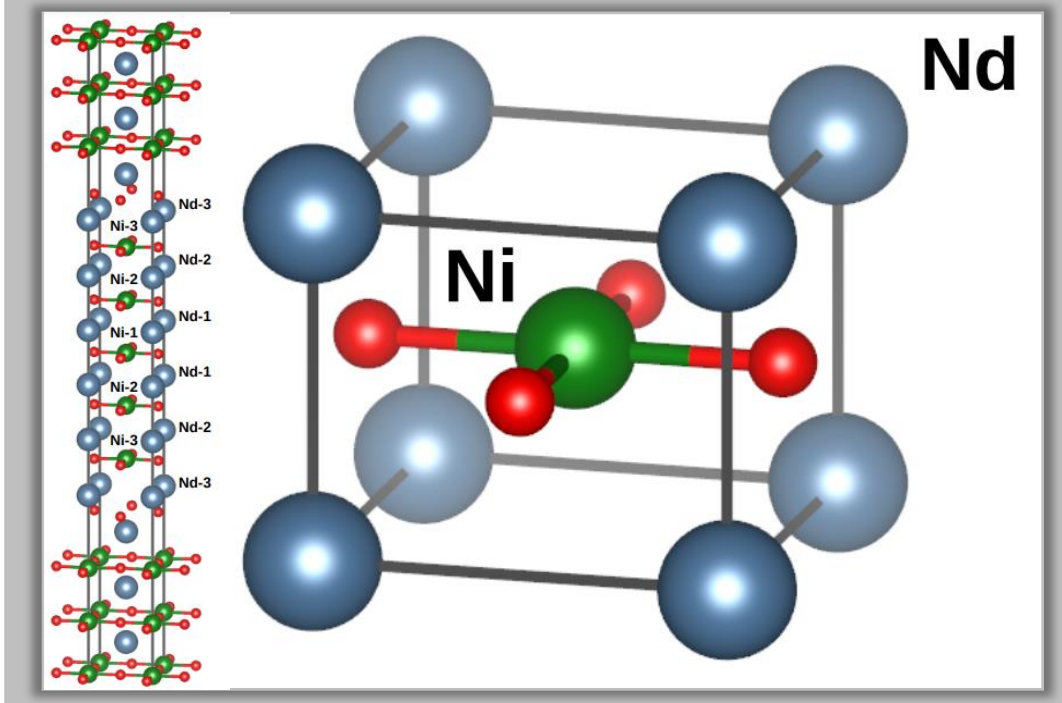

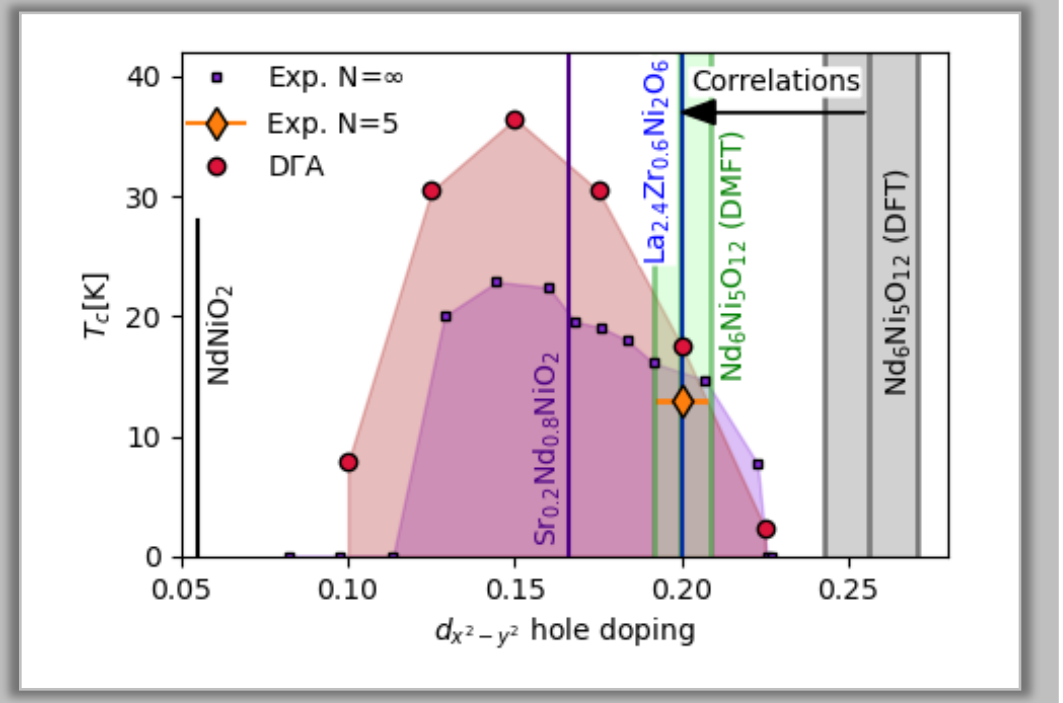

Unraveling strongly-correlated materials' properties with noisy quantum computers

Pauline Besserve – 2nd year PhD student

Atos Quantum Laboratory, Les-Clayes-sous-Bois, France

Centre de Physique Théorique, Palaiseau, France

Advisors: Thomas Ayral, Michel Ferrero

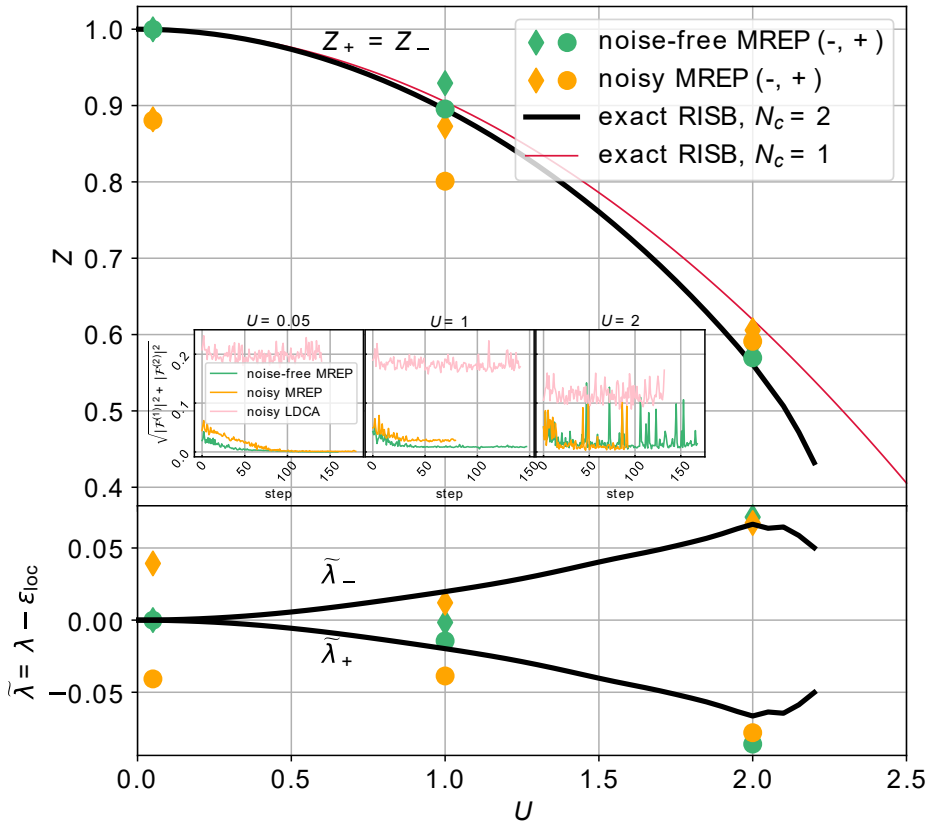

Published in Phys. Rev. B 105, 115108

The effect of short-range antiferromagnetic correlations and Mott physics on the formation of the strong coupling pseudogap

P.-O. Downey[1†], O. Gingras[2,3], M. Charlebois[4], C.-D. Hébert[1], and A.-M. S. Tremblay[1]

- **Mott transition** in the triangular 2D Hubbard model
- **PGs exist** in the triangular 2D Hubbard model
- Neither **long-range** nor **short-range** AFM fluctuations are **linked** to the formation of this strong coupling PG.
- Electron doped and hole doped PGs have a **common origin**.
- The PG is linked to **Mott physics**.

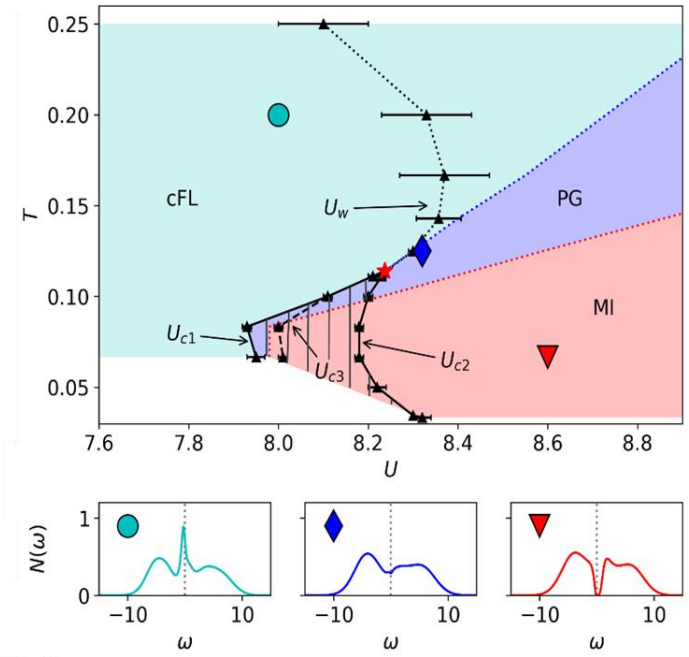

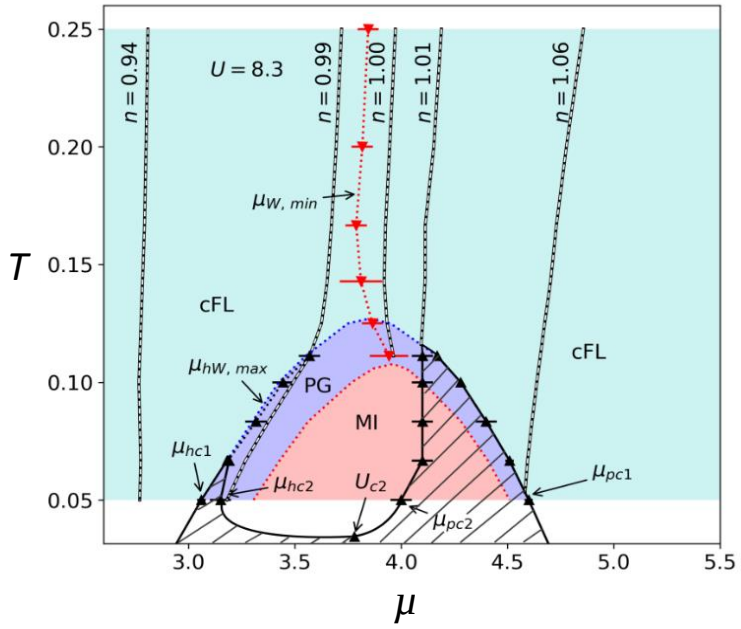

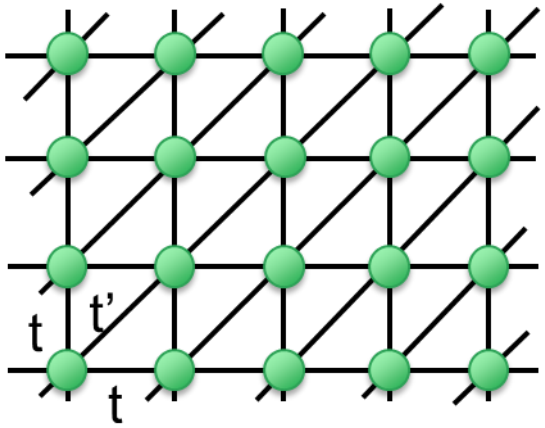

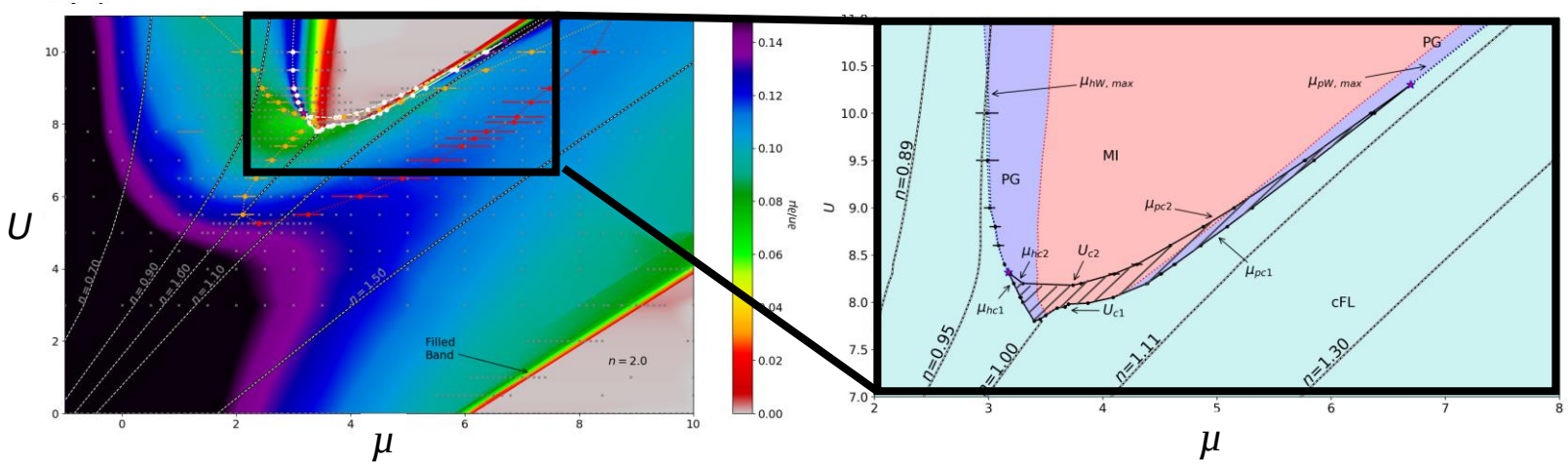

Institut Charles Gerhardt Montpellier

CHEMISTRY: MOLECULES TO MATERIALS

Self Energy functional of the reduced density matrix:

toward a systematic and accurate framework

Quentin Marécat[1], Emmanuel Fromager[2] and Matthieu Saubanère[1]

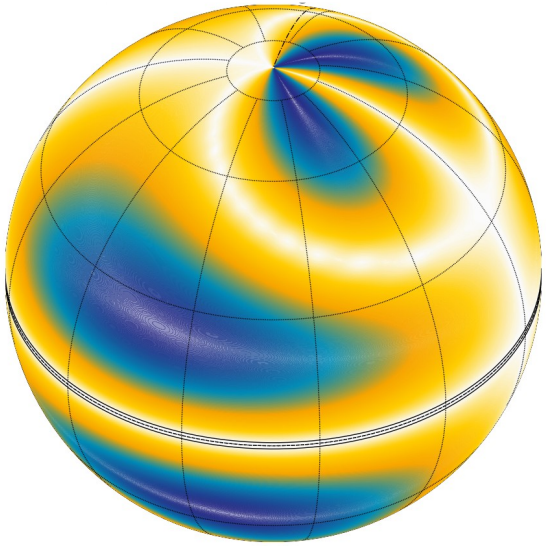

[1] Institut Charles Gerhard Montpellier
[2] Laboratoire de Chimie Quantique, Strasbourg

$SrVO^3$: A multi-tier GW+EDMFT approach

Ruslan Mushkaev, University of Fribourg, Switzerland

- A numerically tractable computational scheme free of ad-hoc parameters
- Consistency check of the multi-tier scheme for $SrVO^3$ in different model spaces
- Plasmons or Hubbard bands? Screening role of Oxygen bands?

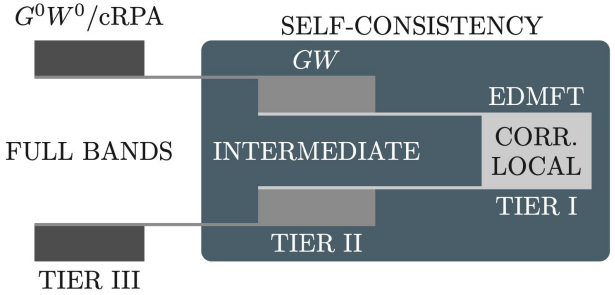

L. Boehnke, F. Nilsson, F. Aryasetiawan, and P. Werner, PRB **94**, 201106(R) (2016)

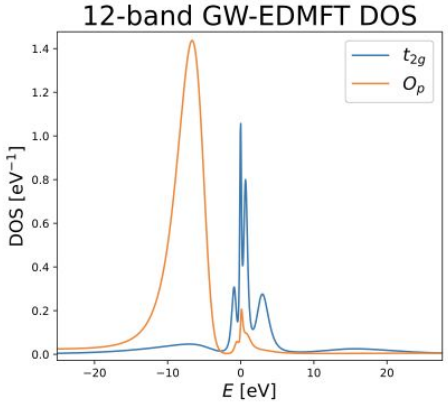

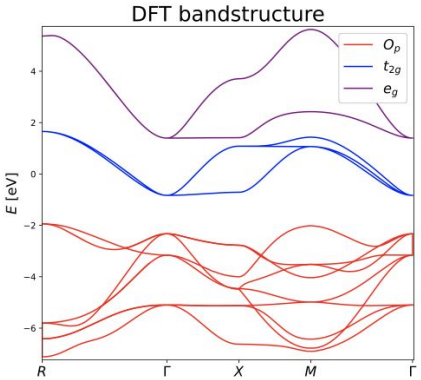

TECHNISCHE UNIVERSITÄT WIEN
AG TOSCHI

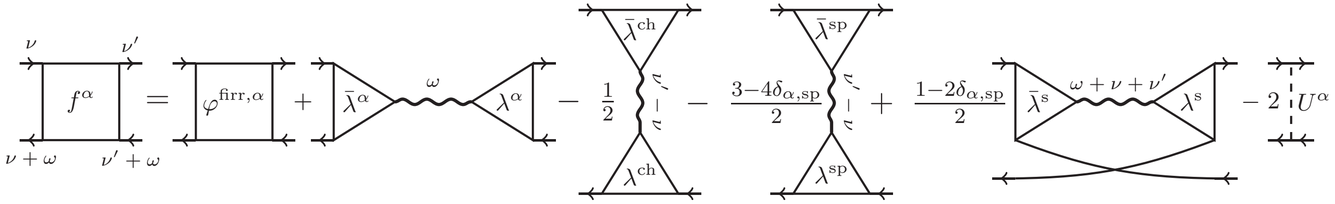

Julius-Maximilians-UNIVERSITÄT WÜRZBURG
AG SANGIOVANNI

Non-perturbative intertwining between spin and charge correlations: A "smoking gun" single-boson-exchange result

$$\chi^{\mathrm{ch}}_{\nu,\nu'} \approx -\beta g^2_\nu \delta_{\nu,\nu'} + -g^2_\nu \phi^{\mathrm{irr}}_{\nu,\nu'} g^2_{\nu'} + \frac{3}{2} g^2_\nu \lambda^{\mathrm{sp}}_{\nu,\nu'-\nu} \omega^{\mathrm{sp}}_{\nu'-\nu} \lambda^{\mathrm{sp}}_{\nu,\nu'-\nu} g^2_{\nu'}$$

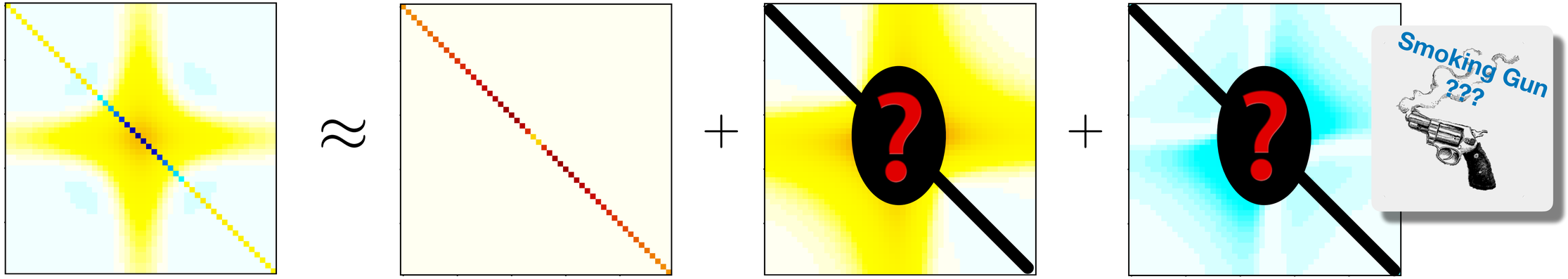

Severino Adler

June 2022, Quebec

Multipolar Order and Quantum Criticality in d^2 Mott Insulators

Sreekar Voleti, Arijit Haldar & Arun Paramekanti
Department of Physics, University of Toronto

Introduction

- **Multipolar Ordered Phases** occur in systems where the symmetry-breaking order parameter is a higher rank multipole of magnetically active ions on a lattice.
- Heavy d-ion materials have large spin-orbit coupling (SOC), which interplays with electron-electron interactions to give rise to interesting physics.
- The nature of multipolar order in $5d^2$ Double Perovskites has been hotly debated, with proposals for Ferro-Octupolar (FO), Antiferro-Octupolar (AFO), and Antiferro-Quadrupolar (AFQ) ordered phases gaining steam.
- We seek to clarify the nature of this multipolar order.

Local Hamiltonian

On a single site, we consider the Hamiltonian for a d^2 ion in an octahedral environment, involving crystal field effects (H_{CEF}), spin orbit coupling (H_{SOC}), and interactions (H_{int}):

$$H_{\text{loc}} = H_{\text{CEF}} + H_{\text{SOC}} + H_{\text{int}} \tag{1}$$

where the electron-electron interactions are of Kanamori form:

$$H_{\text{int}} = U \sum_{\alpha} n_{\alpha\uparrow} n_{\alpha\downarrow} + \left(U' - \frac{J_H}{2}\right) \sum_{\alpha>\beta} n_\alpha n_\beta - J_H \sum_{\alpha\neq\beta} \mathbf{S}_\alpha \cdot \mathbf{S}_\beta + J_H \sum_{\alpha\neq\beta} c^\dagger_{\alpha\uparrow} c^\dagger_{\alpha\downarrow} c_{\beta\downarrow} c_{\beta\uparrow}.$$

The low energy manifold of this Hamiltonian is given by a weakly split $J = 2$ moment into a **non-Krammers ground state E_g doublet**, and an excited T_{2g} triplet[2]. The pseudospin-1/2 ground state doublet, given by

$$|\psi_{g,\uparrow}\rangle = |0\rangle; \quad |\psi_{g,\downarrow}\rangle = \frac{1}{\sqrt{2}}(|2\rangle + |-2\rangle),$$

has dipole matrix elements vanish and higher rank multipoles play the role of the (pseudo)spin operators:

$$(J_x^2 - J_y^2) \sim \tilde{S}_x \quad \text{[Quadrupole]} \tag{2}$$

$$\overline{J_x J_y J_z} \sim \tilde{S}_y \quad \text{[Octupole]} \tag{3}$$

$$(3J_z^2 - \mathbf{J}^2) \sim \tilde{S}_z \quad \text{[Quadrupole]} \tag{4}$$

where the overline in Eq. (3) corresponds to symmetrization. The $\tilde{S}_x$ and $\tilde{S}_z$ quadrupoles together form an XY-like order parameter $(\tilde{S}_x, \tilde{S}_z)$, and the $\tilde{S}_y$ octupole acts like a $\mathbb{Z}_2$ Ising-like order parameter. **Pseudospin ordering in this system hence directly corresponds to ordering of multipoles.**

References

[1] S. Voleti, et al, Phys. Rev. B 104, 174431 (2021)
[2] S. Voleti, et al, Phys. Rev. B 101, 155118 (2020)
[3] A. Paramekanti, et al, Phys. Rev. B 101, 054439 (2020)
[4] D.D. Maharaj, et al, Phys. Rev. Lett. 124, 087206 (2020)
[5] D. Bravyi, et al, Annals of Physics 326, 2793 (2011)
[6] D. Churchill and H.Y. Kee, Phys. Rev. B 105, 014438 (2022)

Two Site Exact Diagonalization

A two-site model with a copy of H_{loc} on each site and a hopping Hamiltonian H_T^γ along a γ-plane bond (shown schematically in Figure 1 for $\gamma = xy$) has a numerically manageable Hilbert space size, and can hence be **solved exactly**

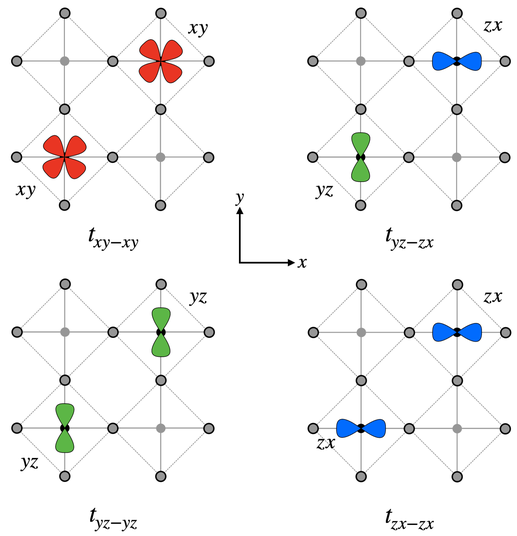

Figure 1: Nearest-Neighbour hoppings in the xy plane in a Double Perovskite lattice. For our problem, the **dominant hopping is t_{xy-xy}**, with all others being subdominant.

We can then use a **Schrieffer-Wolff transformation** [5] to obtain a low energy pseudospin Hamiltonian, which for the $\gamma = xy$ plane, is given by the diagonal form

$$H^{xy}_{\text{spin}} = \mathcal{K}_{Qx} \tilde{S}_{1x} \tilde{S}_{2x} + \mathcal{K}_{Qz} \tilde{S}_{1z} \tilde{S}_{2z} + \mathcal{K}_O \tilde{S}_{1y} \tilde{S}_{2y} \tag{5}$$

Perturbation Theory

The exact solution of the two-site problem is essential to show that **deriving the pseudospin exchange interactions by directly projecting to the ground state doublet is insufficient.**

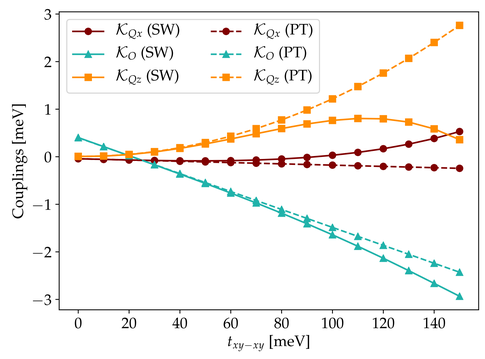

Figure 2: Comparison of Exact Solution with 2nd order Perturbative Calculation. Higher order suppression of the Quadrupolar exchange is evident.

Multipolar Phase Diagram

We observed three distinct multipolar phases when varying the subdominant hoppings from Figure 1: **Ferro-Octupolar (FO)**, **Antiferro-Octupolar (AFO)**, and **Antiferro-Quadrupolar (AFQ)**. We develop the phase diagram by looking at the dominant exchange in Eq. (5), as well as using Monte Carlo simulations on an fcc lattice.

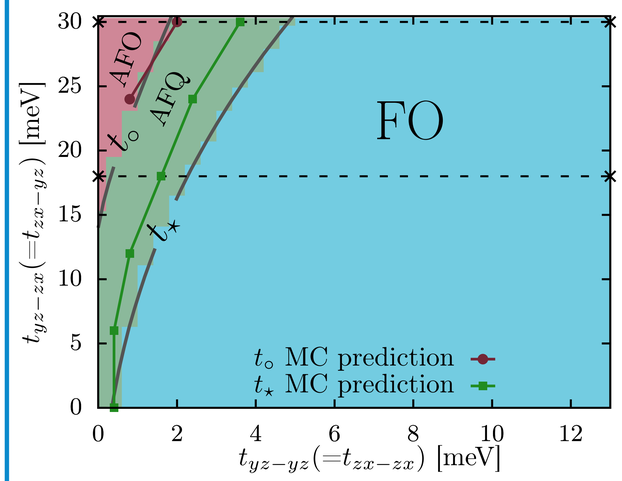

Figure 3: Phase Diagram in the subdominant hoppings using a fixed $t_{xy-xy} = -150$ meV. It can be seen that there is a large swath of FO order, with smaller slivers of AFO and AFQ orders.

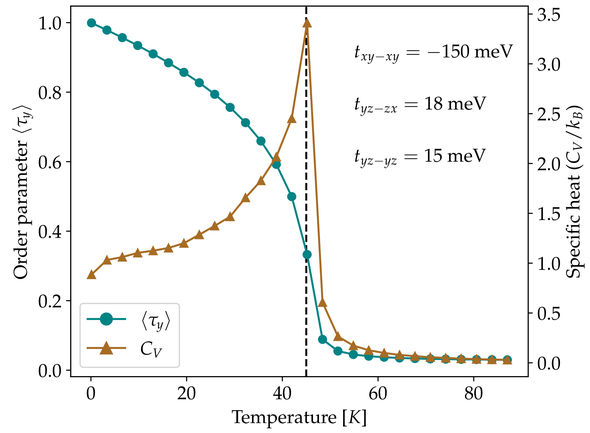

Figure 4: Single phase transition into an octupolar ordered phase, observed in Monte Carlo (MC)) simulations at $T \sim 45$ K using hopping values derived from DFT studies [6]. This is in excellent agreement with experimental observations [4,5]

Tuning to an Ising Quantum Critical Point

By breaking cubic symmetry, we can generate time-reversal even "fields" to the pseudospin Hamiltonian in Eq. (5). Since the octupolar operator (Eq (3)) acts as an Ising-like $\mathbb{Z}_2$ order parameter, this gives us an effective **Transverse Field Ising Model**. Tuning the symmetry breaking fields may allow us to access a **Multipolar Ising Quantum Critical Point (QCP)**. We study two methods for breaking the cubic symmetry - applying strain on the sample, and by reducing the number of layers in the sample along a certain direction.

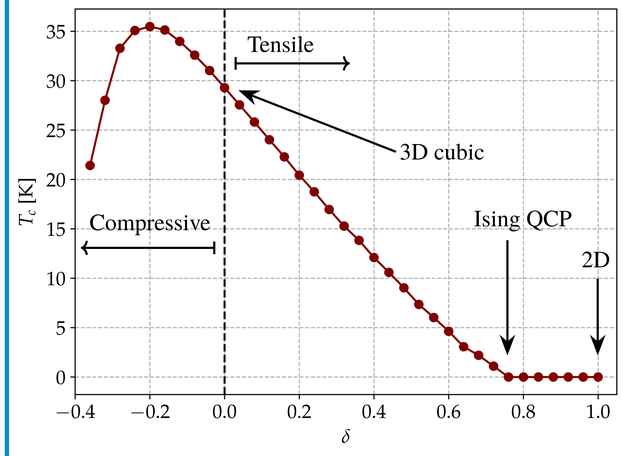

Figure 5: Strain tuning of multipolar order. Applying tensile strain can suppress the critical temperature T_c, allowing one to access an Ising QCP.

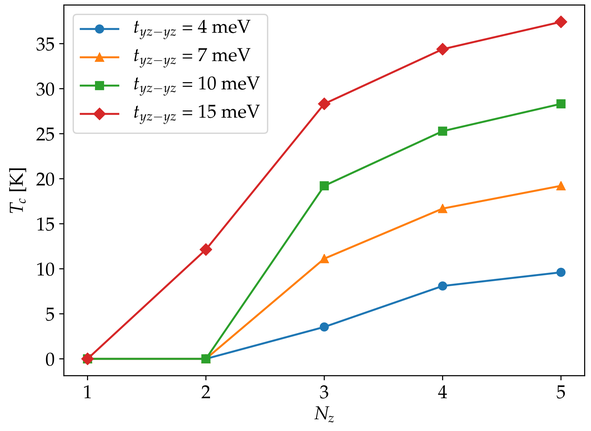

Figure 6: Thin film tuning. The critical temperature can be suppressed by tuning the number of sample layers to two (bilayer sample)

Conclusion

Clarification of the mocroscopic nature of octupolar order in $5d^2$ Double Perovskites, and ways to tune to an Ising QCP.

Superconductivity in simple cubic phosphorus:

The role of dynamical screening and electronic correlations

Viktor Christiansson

University of Fribourg, Switzerland

- Peculiar experimental pressure dependence of T_c
- Theoretical T_c from parameter-free DFT for superconductors (SCDFT)
- Dynamically screened interaction from state-of-the-art many-body methods
  - RPA, GW, GW+EDMFT
- GW quasiparticle energy corrections